University of Alberta

CHEMICAL TUNABILITY OF GLANCING ANGLE DEPOSITION THIN FILMS

by

Shufen Tsoi

A thesis submitted to the Faculty of Graduate Studies and Research in partial fulfillment of the requirements for the degree of **Master of Science**

Department of Electrical and Computer Engineering

Edmonton, Alberta
Spring 2006

Your file Votre référence
ISBN: 0-494-13900-5
Our file Notre référence
ISBN: 0-494-13900-5

Abstract

The first application of siloxane-based chemistry for tailoring the surface chemistry of highly porous, nanostructured thin films fabricated using glancing angle deposition (GLAD) is described. Here, utilizing solution and vapour-phase surface functionalisation methodologies, a chemical dimension is introduced to the tunability of various GLAD nanostructures fabricated with different materials. In particular, efforts were made to convert the originally hydrophilic film surfaces to hydrophobic and superhydrophobic states. The effectiveness of the two surface functionalisation methodologies is demonstrated and compared in this thesis. The functionalised nano-constructed GLAD films demonstrated a high degree of tunability over both structural and surface properties. Specific applications of the functionalised nanostructures are also discussed briefly, along with suggestions for future experiments and potential applications. Without doubt, functionalised GLAD films are well suited for many applications, and the chemical tunability of these films has better the opportunities for further exploration with the GLAD technique.

Acknowledgements

First of all, I owe many thanks to both Dr. Sit and Dr. Veinot. Dr. Sit, you were the first one to introduce me to fabrication of thin films, and without you I would not be writing this thesis. Dr. Veinot, you give me the first introduction to organic chemistry and taught me all the chemical processing techniques I needed for the completion of this thesis and degree. Whenever obstacles appeared, you were there to provide me with your insights and wild ideas, which never fail to help me stumble upon great results. Thus, I am much indebt to both of you and I would have never been able to finish this thesis without all of your knowledge, support and ideas.

I would also like to thank each and every member of the glancing angle deposition group (Andy, John, James, Peter, Mark, Doug Gish, Doug Vick, Jim, Jason, Matt, Bryan, Nick, Anastasia and Dr. Brett), as well as Dr. Veinot's group (Enrico, Colin, Shaun, De-ann, Janet, and Vicky). You always taught me what I need to know, and helped me with insights and ideas whenever it was necessary. What's more important, all of you were always there to assist me when I needed it the most, regardless if it was computer problems, equipment or a chemical experiment.

Special thanks to George Braybrook, who is essential to this thesis because he captured all the amazing SEM images within these pages, and Wayne Moffat, who was always patient and helpful in providing me with the best FTIR results despite the crazy samples I make him analyze. Both of you have given me great advice and suggestions in every characterisation step of my samples. Also essential is Stephanie Bozic, Aruna Kroetch, and Shane McColman, who taught me many vital thin film processing techniques in the University of Alberta's nanofabrication facility.

Now I extend all my gratitude towards my parents who has taught me everything I

needed to know from my first words to how to live. For all of your moral support, financial support and great cooking (especially my father), thanks. Mom and dad, you made the most important contributions in my life and there is no words to express my gratitude towards you.

Finally, to everyone that have encouraged, supported and helped me in anyway, even if it was just a simple smile or a chat at the right time, thanks!

Contents

List of Tables

List of Figures

List of Symbols

α	Flux incidence angle measured from the substrate normal
β	Column inclination angle of thin films
ϕ	Substrate rotation coordinate that is normal to and passing through the centre of the substrate
θ^*	Intrinsic contact angle on a flat surface
θ'	Apparent contact angle on a rough surface
θ_a	Advancing contact angle
θ_r	Receding contact angle
θ	Measured advancing aqueous contact angle
γ_{lv}	Liquid-vapour surface tension
γ_{sv}	Solid-vapour surface tension
γ_{sl}	Solid-liquid surface tension
f	The fraction of solid-liquid interface area in contact angle measurements
H	Contact angle hysteresis
r	Surface roughness factor

List of Abbreviations

CA	Contact angle
CV	Cyclic voltammogram
CVD	Chemical vapour deposition
EB-PVD	Electron beam physical vapour deposition
FTIR	Fourier Transform infrared spectroscopy
LC	Liquid crystalline materials
PVD	Physical vapour deposition
RIE	Reactive ion etching
SA	Self-assembly
SAM	Self-assembled monolayer
SEM	Scanning electron microscopy
VOC	Volatile organic compounds
XPS	X-ray photoelectron spectroscopy

1 Introduction

1.1 History of and recent developments on thin films

For the past century, the versatility and utility of thin films have been exploited in every possible field and industry, ranging from potato chip package coatings and decorations to various biological, optical, electrical, chemical, mechanical, and thermal applications. A thin film is simply a coating deposited on the surface of a material in order to change the properties of the original material. This coating may be composed of many type of materials including metals, alloys, organics, polymers, molecular compounds or any combination thereof. However, there is no straightforward definition that differentiates a "thin" film a "thick" film. The "thinness" in thin films can be defined by either the type of film properties utilized in an application (*i.e.*, surface properties vs. bulk properties) or how the film is fabricated (*i.e.*, depositing individual atoms or molecules vs. particles). Regardless of the definition, thin films have been in existence ever since Egyptian craftsmen beat gold beads into sheets less than 1 μm thick to coat ornamental items with a thin film of gold thousands of years ago. Hence, in the early era of thin films, the sole application of thin films has been in decorative ornaments and jewels. The modern development of thin film technology was considered to be first initiated by Faraday in the mid 19^{th}

century when he exploded thin metal wires in an inert atmosphere [1]. Soon after, Nahrwold in 1887 [2], and subsequently, Kundt in 1888 [3] facilitated the first evaporation of thin films by implementing a vacuum atmosphere to measure the refractive indices of metal films. Subsequently, the technological applications of thin films have continuously increased, especially in the optics and microelectronic industries. From this point on, vacuum technologies along with the various techniques used to fabricate thin films such as physical vapor deposition (PVD) [4–6] and chemical vapour deposition (CVD) [7, 8] have been extensively studied by many researchers. The effectiveness of these thin films in the microelectronics and optics industries resulted in significant improvements in thin film processing methodologies leading to thoroughly developed thin film processes known as microtechnolgy. The term "microtechnology" was developed in the latter half of the century to refer to thin film fabrication and processing techniques that created devices at the micrometer size scale. To satisfy consumers' demand for smaller, better, and cheaper devices in the microelectronics industry, researchers and companies worked together to advance the fabrication and processing techniques from the micro-scale to the nano-scale at an exponential pace. Consequently, microtechnology became what is the most feverish studied topic today, nanotechnology. The modern application and development of nanotechology can be seen in a wide variety of products and research projects including genetic engineering [9, 10], disease detection [11, 12], biosensors [13–15], molecular transistors [16–18], organic light-emitting diodes (OLED) [19–21], photonic crystals [22, 23] and volatile organic compound sensors [24].

1.2 Motivation

Many of today's applications of thin films arise from the ability to exploit the bulk and surface properties of a wide range of thin film materials for material modification purposes. Traditionally, thin films were deposited with the substrate orientated normal to the incoming source flux, and the film properties were dependent on the choice of material, physical film thickness, and the deposition conditions. However, the traditional substrate orientation provides limited control over these variables and nearly no control of the film structure and density. In contrast, by depositing at highly oblique angles measured from

the substrate normal, porous thin films can be fabricated with accurately controlled micro- and nano-structure. This additional degree of control provides another powerful means of tailoring the film's properties for future device applications as well as improving current devices.

Glancing angle deposition (GLAD) is an advanced thin film deposition technique implemented to produce a variety of nanostructures at highly oblique deposition angles. Most of the critical components of the GLAD technique had been documented well before the actual implementation of GLAD. For example, Holland [25] reported extreme oblique angle deposition before 1953 and substrate rotation was investigated by Young and Kowal in 1959 [26]. In 1989, Motohiro and Taga discussed alternating azimuthal deposition angles [27], and other anisotropy effects have been reported by various research groups [28–30]. In 1995, Robbie and Brett combined all of these features into a well-controlled, single system classified as glancing angle deposition that could accurately engineer porous nanostructures [31]. The extreme oblique angle of incidence (>80°), and the structural and porosity control that GLAD provides set it apart from all other oblique angle deposition methods. Since then, the GLAD technique has provided a foundation for a great amount of other work.

Currently, many research groups are simultaneously investigating aspects of the GLAD technique. Arnold *et al.* have investigated the optical behavior and effects of chiral thin films deposited at oblique angles [32]. Very recently, photonic filter properties of these films have been examined by Hodgkinson *et al.* [33]. Lakhtakia has proposed various theoretical photonic crystal modes [34], and spectra hole functions for optical fluid sensor applications [35] of GLAD-like thin films as well. Fan *et al.*, from University of Georgia, have recently investigated wettability of GLAD films as a function of film thickness [36, 37]. In addition, recent developments of the GLAD technique [38] and combinations of GLAD and other thin film processes such as direct write lithography [39, 40] have further improved the control GLAD provides and allow devices to be fabricated for a wide range of applications including three-dimensional photonic crystals [41], band-pass rugate filters [42] and sensors [43, 44]. Though GLAD films are well-suited for many applications, two of the most promising applications for these porous, high surface area

films are chemical sensing and optical devices. To realize optical and sensing devices with optimal performance, the ability to control the interaction of the film material with its surrounding environment is essential.

Chemical sensors require high selectivity to discriminate between different substances in their surroundings, while at the same time, they also need to have high sensitivity towards the substance to be detected. In contrast, many optical devices must be inert to environmental changes since these changes can cause shifting of the device response. For example, a optical bandpass filter must be resistant to humidity changes in the atmosphere because the position of the pass band may be dependent on relative humidity. Thus, to control the device interactions with the environment, it is necessary to develop methods for tuning the hydrophobicity or hydrophilicity of thin films. In general, there are two main properties that influence hydrophobicity or hydrophilicity of a material: 1) the surface structures or roughness, and 2) the surface chemistry. It has been demonstrated by other researchers [36] that hydrophobicity of the GLAD films has a dependence on aspect ratio (*i.e.*, the height to width ratio of a structure) and thus, some control over its interactions with solvents could be achieved by varying surface roughness and film thickness. However, this structural approach to controlling the wettability of the film surface is limited as it provides no control over the chemical response of the film. This thesis examines chemical functionalisation methods as a means to tailor the surface chemistry of these unique GLAD films and demonstrates the ability to add yet another dimension of control, *i.e.*, chemical tunability, to GLAD.

1.3 Scope and Organisation of this Thesis

As all of the work reported here is based on thin film technology and glancing angle deposition, I first give an overview of thin film technology and the history and development of GLAD in the remainder of Chapter 1. I then proceed to a description of the general concepts of oblique angle deposition, in particular the GLAD technique practiced in this research, and examples of applications of GLAD films.

Chapter 2 provides background information on organic thin films used in tuning the surface chemistry or surface properties of materials. Different types of organic thin films

and the principles behind the formation of these films are introduced along with examples of applications for the various types of organic thin films. In particular, general concepts, recent developments, and applications of the self-assembly (SA) technique are discussed in more detail. Finally, the utility of organic thin films in controlling the wettability of a material is provided.

The basic experimental design for tailoring the surface chemistry of various GLAD films is detailed in Chapter 3. Specific information on the material and parameters used to fabricate the GLAD films for the present studies are reported. Also included in this chapter are details on processing of as-deposited GLAD films using oxygen plasma reactive ion etch (RIE) and surface functionalisation techniques. Results on characterisation of GLAD films treated by RIE for various lengths of time are reported, as well as the procedures for solvent-based and vapour-phase surface functionalisation.

Characterisation results of pre- and post-functionalisation SiO_2 GLAD films are discussed in Chapter 4. In this chapter, the attachment of organic moieties to the surface of the GLAD film and its effects on the surface chemistry of the film are investigated. The ability of chemical reagents to penetrate the porous GLAD structure and successfully tailor the surface chemistry of the structures is demonstrated.

In Chapter 5, effects of solvents on the GLAD film structures are examined. Subsequently, vapour-phase functionalisation is implemented in an attempt to eliminate the use of solvents and their potentially detrimental effects on the nanostructures. The utility of solution and vapour-phase functionalisation methods to tune the surface chemistry of metal oxide GLAD films are evaluated and compared.

Finally, application of surface-treated GLAD film to a humidity sensor and an optical filter is demonstrated in Chapter 6. This chapter also includes the summary, conclusions, potential applications of surface-treated GLAD, and recommendations on future research to further develop and apply the chemical tunability of various types of GLAD films.

1.4 Deposition Techniques of Thin Films

As mentioned before, there are numerous methods for fabricating thin films, and the choice of method depends heavily on the type of material and its properties. Thin films can be

created by methods such as dip-coating, where the substrate is simply immersed into a bath containing the desired coating and then extracting it from the same bath. This method tends to produced films with questionable uniformity; however, if uniformity is of importance, a spin-coating method can be used. As the name implies, the desired coating is spun onto a substrate at a pre-defined speed. In this case, the user has some control over the thickness of the film and the uniformity via the spinning speed. There are also many other deposition methods such as sputtering and CVD that have been employed as common practice in industries. Most of these methods provide the user with more control over the thickness, structure and uniformity of the film. A detailed description of each deposition technique is outside the scope of this thesis since the majority of thin films in this work were fabricated using electron beam evaporation. This process is described in detail in the next section.

1.5 Growth Mechanics of Evaporated Thin Film at Normal Incidence

Electron beam physical vapour deposition (EB-PVD) is a directional deposition technique performed in an evaporator. Electrons generated through thermionic emission from a heated tungsten cathode. These electrons are accelerated by a high voltage, typically ranging from 6 to 20 keV, and passed through a hole in the anode. A magnetic field from permanent magnets is used to direct and focus the electron beam onto a water cooled crucible containing a pocket filled with evaporant material. Electromagnetic coils can deflect the electron beam allowing it to be scanned over the whole evaporant surface [5,45].

At the crucible, energy from the electron beam is transferred to the crucible contents, heating them while increasing the vapour pressure of the evaporant. When the vapour pressures of the evaporant increases to a point at which appreciable kinetic energy is gained by the atoms, they escape into the vapour phase, ultimately forming a gaseous flux. To minimise collisions between ambient gas molecules and the evaporated atoms, EB-PVD is performed in a high vacuum environment such that the mean free path of the particles is sufficiently large. This implies the majority of evaporated flux from the crucible will follow a straight-line trajectory such that any objects in the direct line of sight between the crucible and the interior of the vacuum chamber are bombarded [46]. The amount

of mass deposited on a surface has a cosine dependence on geometry, with maximum deposition occurring directly above the source. Consequently, the substrate, whose surface is to be coated, is positioned in the direct line of sight from the crucible and oriented normal to the evaporation source such that maximum deposition is encouraged. A crystal thickness monitor (CTM) is placed at close proximity to the substrate and its surface is orientated such that it is in the direct line of sight of the vapour flux (as illustrated in Figure 1.1) to produce a reasonable, reliable estimate of the film thickness at the substrate. The CTM consist of a quartz crystal which oscillates at a frequency with approximate linear dependence on the mass, and hence the thickenss, of the film deposited onto its surface [47]. By measuring the difference between the reference resonant frequency and the oscillation frequency after the deposition of the mass, the mass and thickness of the film on the crystal can be calculated and related to the deposition rate at the substrate. A simplified traditional, normal incidence thin film deposition system is illustrated in Fig. 1.1 showing all the important elements inside the system .

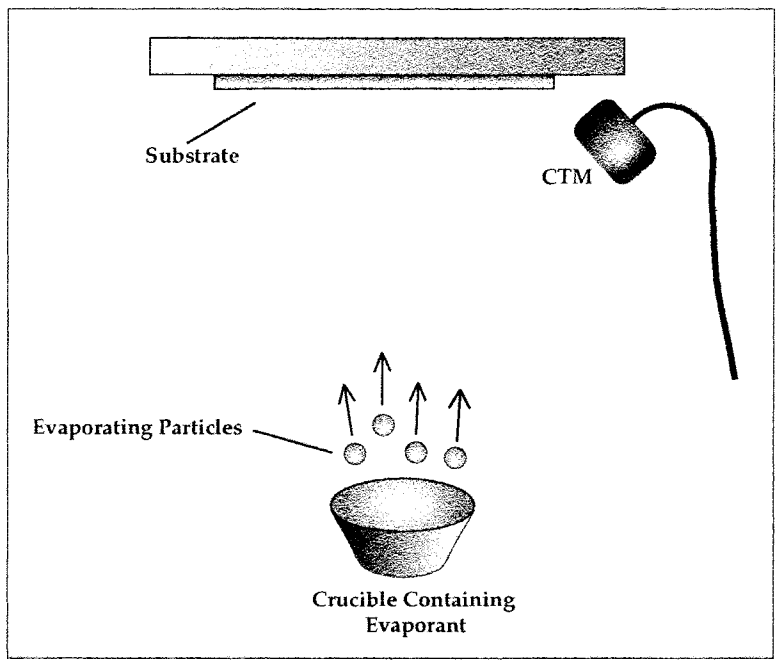

Figure 1.1: Traditional electron beam evaporation system. Evaporated atoms are ejected from the heated evaporant inside the crucible and follow a line-of-sight trajectory until they strike the crystal thickness monitor (CTM) or the substrate surface at normal incidence.

Generally, atoms striking the substrate surface can behave in three ways: 1) adhere

permanently to the substrate, 2) adhere to the substrate for a short time and then re-evaporate into the vacuum chamber, or 3) reflect immediately from the substrate. In the most important case, particles physisorbed on the substrate surface tend to diffuse a short distance before settling in a local minimum energy site [48]. The diffusion distance of the adsorbed atoms, refer to as adatoms, is determined by the melting temperature (or the vapour pressure) of the evaporant, the substrate temperature, and the energy of the impinging particles. Gaseous particles produced from substances with higher melting points will have a shorter average migration distance before permanently sticking to the substrate than lower melting point materials. Note that this diffusion distance is important to the GLAD concept and quality of the GLAD films.

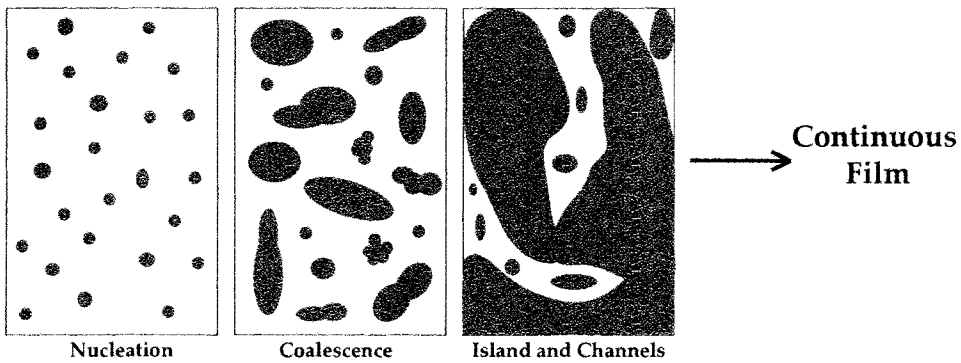

Figure 1.2: Stages of formation for a normal incidence thin film. At the early stage of growth, atoms minimize their surface energy by clustering to form nuclei. The nuclei then coalesce into larger particles. These particles encounter each other and form large islands leaving only holes and channels until a continuous film is created.

During the random diffusion process, adatoms tend collide with each other and form clusters known as nuclei. Small nuclei may not be stable and are usually prone to re-evaporation until a critical, stable size is reached. However, because two particles colliding or in contact with each other will have lower potential energy than two separate atoms, the formation of nuclei will reduce the overall potential energy of the adatoms and the growing film. As a result, adatoms impinging on the substrate surface thereafter will tend to adhere to the existing nuclei rather than forming new nuclei. The critical size refers to the minimum size below which, the nuclei are unstable and will re-evaporate into the vacuum chamber. Once the critical size is reached, the nuclei continue to expand outwards

from their centres, and eventually grow sufficiently large for them to encounter each other and coalesce into one large island. Nucleation will continue to proceed on freshly exposed areas as large islands expand, leaving only channels or holes of uncovered area. Ultimately, the islands will agglomerate and expand to a sufficient degree to form a continuous film. The four stages of thin film growth are illustrated in Fig. 1.2.

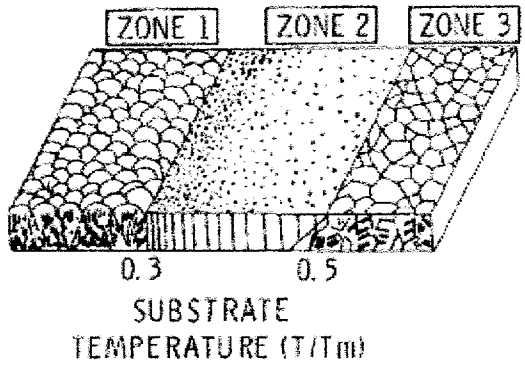

Figure 1.3: Structure zone model for evaporant materials developed by Movchan and Dimchishin. T refers to the substrate temperature and T_m is the melting temperature of the evaporant. Zone 1 classifies film structures with dome shaped tops separated by void boundaries as a result of atomic shadowing. Films in zone 2 have a smooth appearance with columnar grains separated by intercrystalline boundaries. Zone 3 defines film structures that are crystalline with properties similar to annealed films and yields activation energy corresponding to bulk diffusion of the material. This image is obtained from [49].

There are three growth mechanisms which determine thin film growth as well as structure: surface diffusion, bulk diffusion, and atomic shadowing. The first two are uniquely thermal processes reliant on substrate temperature as well as the melting point of the material as mentioned above. Structure zone models (SZM) that classify the film structure and crystallinity according to substrate temperature and deposition pressure have been proposed for both evaporated [49] and sputtered [50] thin films. A more developed, revised SZM has also been proposed, which provides more insight on thin film morphology and growth under a wide range of deposition conditions [51, 52]. According to the SZMs, higher temperatures lead to greater bulk and surface diffusion and result in a more crystalline film with fewer defects. Atomic shadowing, the other main growth mechanism, arises from the three-dimensional nature of the growing nuclei and is dependent on

the deposition geometry. This last process is essential to the fabrication of porous nanostructured GLAD films, which will be described in the following sections. For thin films deposited at normal incidence, atomic shadowing is minimal and surface diffusion is the predominant effect, resulting in a continuous film with a structure described by zone 1, 2 or 3 of the structural zone model (Fig. 1.3) depending on the substrate temperature.

1.6 Glancing Angle Deposition

1.6.1 Oblique angle deposition

For oblique angle deposition, the initial nucleation stage of thin film growth proceeds as described previously. However, as the nuclei grow, they begin to cast a shadow behind themselves as a result of their three-dimensionality. These shadows form restricted areas that are not accessible to atoms arriving at an oblique angle. Hence, impinging atoms can only be deposited directly in areas such as the tops and near sides of the nuclei. The atomic shadowing effect is accentuated as the nuclei grow (Fig. 1.4). In addition, the more oblique the deposition angle, the greater the shadow area, and the more restricted the accessible area becomes for the impinging flux. In this situation, there are two offsetting effects in play for molding the thin film microstructures; the self-shadowing of the nucleus prevents incident flux from reaching certain regions while surface diffusion encourages it. If the arrival angle of the incidence flux is sufficiently oblique, and the substrate temperature is relatively low, the surface mobility of adatoms become too low to facilitate filling of the voids or uncovered areas. Thus, the atomic shadowing effect dominates over surface diffusion and porosity is created in the thin film as areas become permanently inaccessible.

1.6.2 Growth Mechanics of GLAD

Glancing angle deposition exploits the growth mechanism of thin films under oblique angle incidence to create porous columnar nanostructures. The deposition angle or the angle of incidence for the vapour flux is measured from substrate normal, and is denoted α. Glancing angle deposition is achieved when the film is deposited at α greater than 80°. Under these deposition conditions, adatom migration on the substrate surface is limited

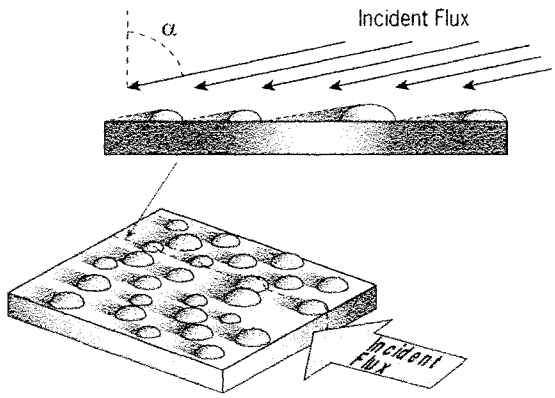

Figure 1.4: Atomic shadowing effect is a result of the three-dimensionality of the nucleus as seen by the vapour flux arriving at an oblique angle at the substrate surface.

and the atomic self-shadowing effect becomes the dominant growth mechanism. The atoms striking the surface of the substrate are then confined to encounter the existing nuclei from only one side, *i.e.*, the side facing the vapour source. Furthermore, when small nuclei are completely engulfed by the shadow of larger structures, these nuclei do not accumulate additional material and their growth is terminated. This concept is referred to as preferential growth where large structures can continue to expand and grow while smaller ones are extinguished. Hence, the structures grow without having all the areas on the substrate covered and a porous columnar film with an inclination towards the vapour flux is produced (Fig. 1.5). The column inclination angle β and porosity of the film are dependent on the flux incidence angle α. For α lower than 60°, changes in column angle arising from a change in the deposition angle can be predicted using the empirically derived tangent rule [53]:

$$\tan\ \beta = \frac{1}{2}\ \tan\ \alpha \tag{1.1}$$

However, at flux incidence angles greater than 80°, which is the case for most GLAD films, this effect is more accurately described by the geometrically derived Tait's rule [54]:

$$\beta = \alpha - \arcsin[\ \frac{1}{2}\ (1 - \cos\ \alpha)] \tag{1.2}$$

In general, the results from these rules show that β is always less than α, and greater flux incidence angles lead to greater column inclination and porosity. The film structure

described in Fig.1.5 is the most basic GLAD structure since the fabrication of all other types of nanostructures use the same principles, but involves substrate rotation.

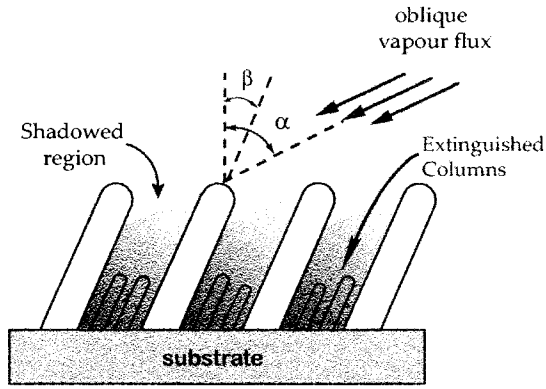

Figure 1.5: When vapour flux arrives at an extreme oblique angle, the smaller columns engulfed inside the shadow of larger columns are extinguished as a result of preferential growth and column competition. The remaining columns grow towards the direction of vapour flux, with an column inclination angle β. This angle is always smaller than the deposition angle α.

1.6.3 GLAD Apparatus and Substrate Motion

To create various types of microstructures, GLAD exploits two main properties of thin film growth. One is the deposition angle α which provides a degree of control over the inclination of columns and the amount of shadowing, which in turn leads to control over the porosity of the thin film. The second is the fact that the inclination of columnar microstructure growth always tends towards the source flux. Thus, by changing the apparent direction of the vapour flux with respect to the substrate through substrate motion, the direction of growth is altered and various microstructures can be fabricated. A schematic of the GLAD apparatus is given in Fig. 1.6. To achieve fine control over the microstructures, directionality of the source flux is required. The substrate is positioned at the greatest feasible distance from the source to achieve the narrowest possible angular distribution of the vapour flux and therefore, directionality. In a common GLAD system, the chuck, which substrates sit on, is positioned 41.5 cm away from the source crucible. Motions of the chuck and thus the substrate are controlled by two stepper motors. One motor controls substrate rotation about the axis parallel to substrate surface, *i.e.*, it adjusts

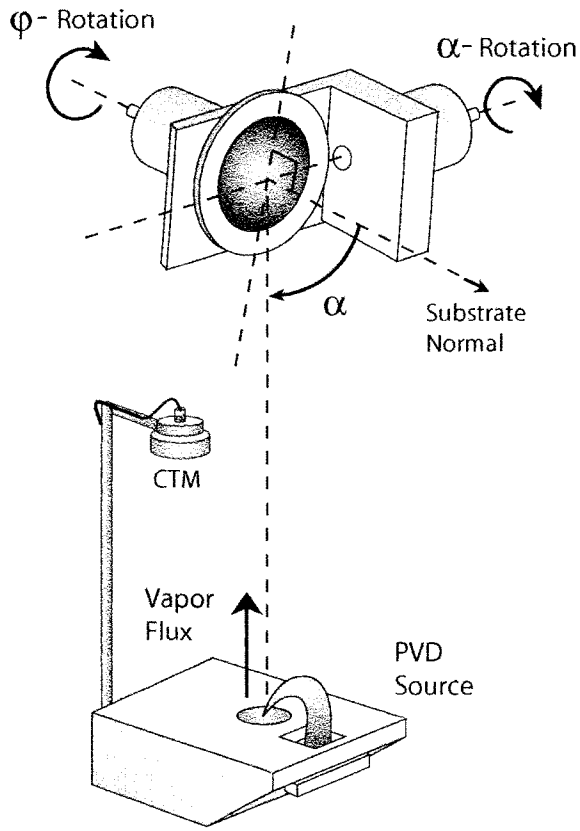

Figure 1.6: A schematic of the glancing angle deposition apparatus.

porosity of the film via α. The second motor controls substrate rotation about the axis normal to substrate surface (ϕ) to adjust the apparent azimuthal direction from which the vapour flux arrives at the substrate. During deposition, the substrate positions in both α and ϕ may be varied continuously according to a set of pre-programmed instructions. Both the speed and length of substrate rotations are determined by user-defined parameters such as thickness and type of microstructure, as well as deposition rates. A great deal of control over the GLAD film morphology throughout the deposition process is thus achieved.

1.6.4 GLAD Microstructures

Slanted post microstructures

One of most basic microstructures produced by GLAD is the slanted post microstructure. No substrate motion is necessary for this type of microstructure. The α motor is maintained at a position based on the desired, but fixed column angle and porosity, while position of

the ϕ motor is arbitrary. Both stepper motors remain stationary in their position throughout the deposition. A schematic illustrating the activity of the substrate and source flux is given in Fig.1.7, as well as an SEM image of a representative GLAD-grown slanted post film. This is a silica film deposited at $\alpha = 85°$ and has a thickness of 500 nm.

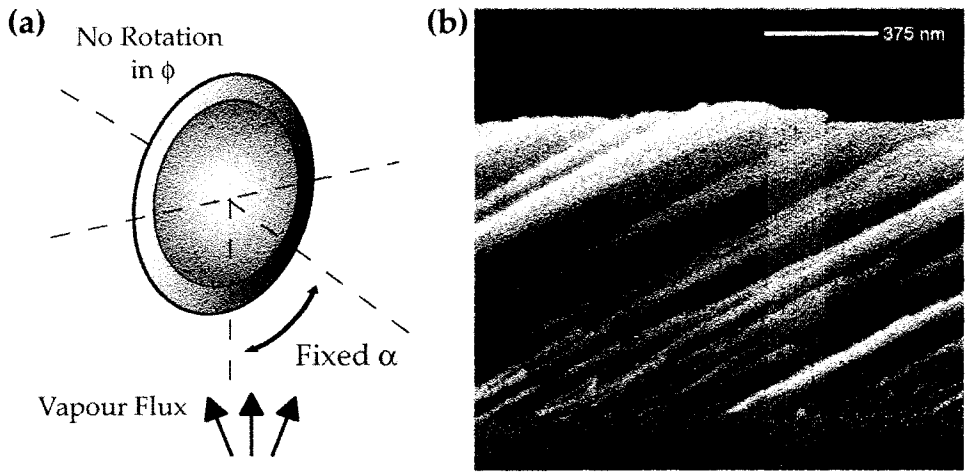

Figure 1.7: (a) Slanted post structures were deposited by maintaining a fix deposition angle α throughout the deposition process. (b) SEM micrograph of slanted post silica structures resulting from the process described in (a).

Helical microstructures

For helical structured columnar film, the substrate is rotated continuously about ϕ. As the substrate rotates gradually, the apparent azimuthal position of the source changes and the columnar structures slowly wind outward from the substrate in a source-tracking manner. The pitch of the helices is determined by the revolution rate of the substrate; the slower the revolution, the greater the pitch. However, a constant revolution rate is not necessarily employed for the production of a constant pitched helical film. A constant rotation can lead to deviations in the helical pitch if there are fluctuations in the deposition rate. To achieve a constant pitch, the revolution rate of the substrate must vary with the deposition rate. In other words, the stepper motor will only move a step forward when a specific thickness has been accumulated on the CTM. This allows the user to specify the helical pitch and fabricate more uniform helical films. A representative SEM image of a helical film and a schematic depicting substrate rotations used to produced a helical film is provided in

Fig.1.8.

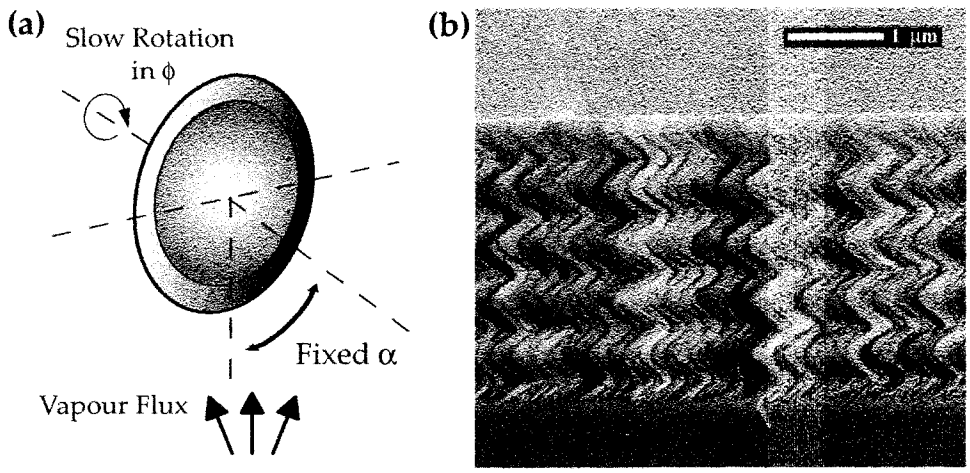

Figure 1.8: (a) Helical structures were deposited by maintaining a fix deposition angle α and slow substrate rotations about ϕ throughout the deposition process. (b)is a SEM micrograph of helical structured alumina film resulting from the process described in (a).

Vertical post structure

Vertical post structures are evolved from the helical microstructure. When the substrate is rotated rapidly about ϕ, the pitch of the helices decreases until, at sufficiently high rotation rates, it becomes indiscernible and the helices degenerate into vertical posts. For most common evaporants, this effects occurs at helical pitches lower than 40 nm. α is held constant throughout the deposition. A SiO_2 vertical post film deposited at 85° is presented in Fig. 1.9 along with a schematic of the substrate motions during deposition.

1.6.5 Summary of GLAD

The simple GLAD structures mentioned above illustrate the significant effect of substrate rotation on thin film structural control at the nanometer scale. Many other complex structures such as graded-index films [42, 55] and self-sealed microchambers [56] can be fabricated by simply steering the direction of columnar growth by varying α and ϕ during deposition. Though these complex structures were not used in this thesis, they are the basis for the realization of many applications. For example, a graded-index GLAD film can be applied as antireflection coating [55], and fine square spiral structures created by

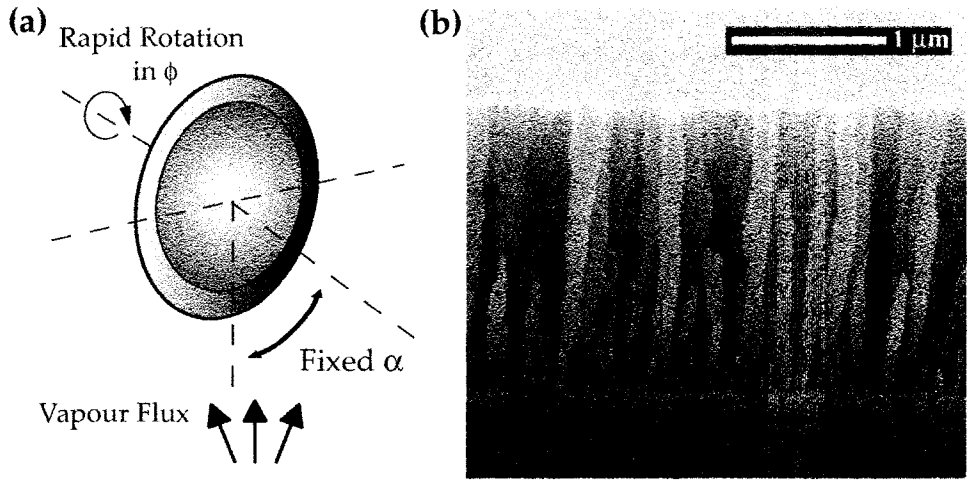

Figure 1.9: (a) Vertical post structures were deposited by maintaining a fix deposition angle α while rotating the substrate rapidly about ϕ throughout the deposition process. (b) SEM micrograph of vertical post silica film resulting from the process described in (a).

GLAD are well suited for the fabrication of three-dimensional photonic crystals [39]. In addition, the porosity and high surface area of these films makes them ideal for sensing and catalytic applications. However, to date, no attempt to tailor or exploit the surface chemistry of these GLAD films has been reported. Hence, the primary intent of this thesis is to add chemical tunability to the degrees of control in the GLAD technique by tailoring the surface properties of GLAD films with surface functionalisation methods and organic thin films.

2

Surface Functionalisation with Organic Thin Films

Today, surface properties of many products such as clothes, windows, and kitchenware have been modified through some form of chemical treatment to produce the final product that is sold in stores. Surface modification has always been essential to mankind because it allows us to combine useful bulk properties (*e.g.*, optical, electrical, *etc.*) of materials with the appropriate or desired surface properties (*e.g.*, wettability, adhesiveness, corrosion resistance, low wear) to develop materials with properties better suited for specific applications. For example, the stability and physical integrity of the metal/semiconductor-organic interfacial cohesion and contact is of vital importance to the performance of an organic light-emitting diode (OLED), and it can be greatly improved by modifying the surface energies of the two contacting materials with an adhesive self-assembled organic layer [57]. Many applications and devices today are reliant on chemical modification techniques to achieve control over surface properties of a wide spectrum of materials. These surface treatment techniques are primarily based on the growth of organic thin films on surface of materials. This chapter provides an overview of the common types of organic thin films and the various methods utilised in the preparation of these films, and

in particular, the methods used to prepare self-assembled monolayers.

2.1 Background

Early studies of organic thin films [58, 59] were centred around macroscopic properties such as wettability and friction due to of the lack of appropriate characterisation tools. With the introduction of microscope-based analytical tools, the field of surface modification was revolutionised. Since then, the great potential of organic thin films for applications in wetting control [60], optical devices [57, 61, 62], sensors [63–66], and various other applications have been discovered and exploited. With the wide range of organic materials and correspondingly wide variety of molecular properties, it is not surprising to find many different types of organic thin films and methods of preparation. One class of organic thin film materials that has become very popular in recent years is polymers, which are generally prepared by spin-coating. However, the study of polymeric thin film is outside of the scope of this thesis since they are not used in any of the work presented here. The focus of this this chapter is on the group of crystalline organic thin films, and the different preparation methods for these films. The following sections will discuss the principal concepts behind some of the most common types of organic thin films and the techniques for preparing such films.

2.2 Different Types and Preparation of Organic Films

2.2.1 Langmuir film

In the 19^{th} century, Langmuir speculated that oleic acid ($C_{17}H_{33}COOH$) forms a monolayer of amphiphilic molecules on water surface by observing various experiments of oils spreading on water [67]. Combined with the previous works of others such as Pockels [68] and Hardy [69], he postulated that the carboxyl group (–COOH) of oleic acid has a marked affinity for water whereas hydrocarbons ($-CH_3$) are insoluble in water and have a greater affinity for each other than water. Hence, a group of oleic acid molecules on water will organize themselves such that the carboxyl groups form hydrogen bonds with water molecules, while the hydrocarbon tails are packed above the carboxyl layer (*i.e.*, sticking

out and away from water molecules). These films were later named after Langmuir. Today, Langmuir films refers to any type of amphiphilic molecules (*i.e.*, molecules with both a polar, water soluble group and a non-polar, water-insoluble hydrocarbon chain) spreading on a hydrophobic or hydrophilic liquid substrate at the gas-liquid interface (Fig.2.1).

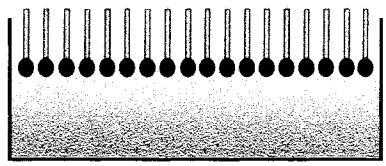

Figure 2.1: Schematic of the formation of a Langmuir film. A monolayer of amphiphilic molecules are formed on top of the water surface at the liquid-gas interface. The ovals represents the hydrophilic polar heads while the rods represent the hydrophobic non-polar tail

2.2.2 Langmuir-Blodgett films

Blodgett first created Langmuir-Blodgett (LB) films by transferring a monolayer of calcium stearate on the water surface to a glass substrate. This was accomplished by first placing a small amount of stearic acid ($CH_3(CH_2)_{16}COOH$) dissolved in benzene onto a water surface containing dissolved calcium salts. The calcium ions then reacts with the stearic acid to form a monolayer of calcium stearate ($(CH_3(CH_2)_{16}COO)_2Ca$) film, where the $-(COO)_2Ca$ head groups are in contact with water and the $-CH_3$ tails are oriented away from the surface of water. Next, the film is compressed mechanically using a barrier such as a drop of oil until the molecules of the film are densely packed and orientated perpendicular to the water surface. Finally, this monolayer is transferred to a glass substrate by dipping the substrate into the film and slowly raising it out of water (Fig. 2.2). As the glass slide is raised out of water, the water must recede from the glass wherever the film attaches itself the solid substrate. Thus, the water shedding behaviour is important in the preparation of LB films, and if the solid substrate was extracted slowly (5 to 10 cm/min.), the substrate should emerge completely dry. Additional layers of the film can be added one at a time by successive repetitions of this procedure [58, 70].

Organic films created by this method are not necessarily chemically bonded to the substrate and hence are not robust and may crack easily. Generally LB films can be

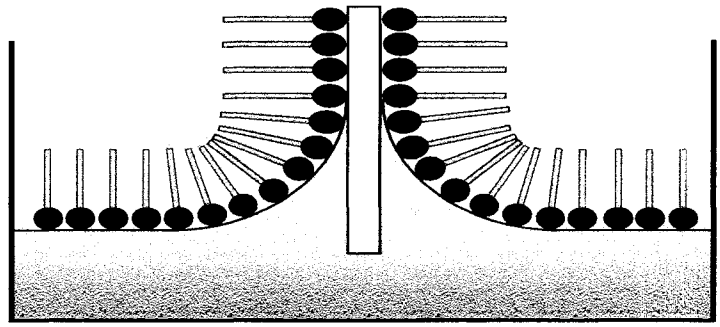

Figure 2.2: Schematic drawing of the formation of a Langmuir-Blodgett film. A Langmuir film can be transferred from the surface of water to a solid substrate by raising the substrate slowly out of the liquid.

removed by rinsing the substrate with aqueous or non-aqueous solvents. It is important to note that the spreading of the film onto the solid substrate depends on the affinity of the molecules' head group towards the substrate (*i.e.*, the head group of the molecule must have a stronger affinity for the solid substrate than the liquid). This concept implies that only selected compounds that form LB films on water can be transferred to a solid substrate intact. Furthermore, it is difficult to produce a highly crystalline and robust monolayer using this method because of the lack of thermal and structural stability.

2.2.3 Organic Molecular Beam Epitaxy

Organic molecular beam epitaxy (OMBE), sometimes referred to as organic molecular beam deposition (OMBD), fabricates ultrathin organic films by vapour-deposition of atoms or molecules in a ultrahigh vacuum environment. The evaporation technique used in this type of system is very similar to the inorganic MBE systems. The uniqueness in this vapour-deposition is it can deposit organic molecules onto reactive and inert substrates. Reactive substrates are generally metals or semiconductors that interact with the deposited organic layer chemically. Inert substrates, as the name implies, do not react with the organic molecules [71, 72]. Graphite and insulators such as silicon dioxide are commonly used as inert substrates. The advantage of vapour-deposition using an OMBE system is the ability to precisely control composition, thickness, structural order and growth temperatures of the organic thin film, as well as providing an extremely clean environment. However, such

systems are highly expensive and there still remains the question of the need for ultrahigh purity in organic thin films since the attraction of most organic thin films stems from the general ease and low cost of fabrication and processing for device applications.

2.2.4 Self-Assembly

Another class of organic thin films is self-assembled monolayers (SAM). The term "self-assembly" in the chemical sense refers to the arrangement of atoms or molecules into an ordered, energetically stable structure without outside intervention [73]. Self-assembly can also involve the aggregation of functional entities towards a stable form. A self-assembled monolayer is an organization of molecules at the liquid-solid or gas-solid interface induced by strong chemisorption (*i.e.*, strong covalent bonding) between the molecule's head group and the substrate. Hence, films prepared by self-assembly are highly crystalline, structurally robust and thermally stable despite that the general concept of self-assembly is very similar to the concepts applied in LB films. Hence, the main differences between a LB film and a self-assembled monolayer are the crystallinity, robustness, and thermal stability of the films [58, 60]. A SAM molecule generally consist of three constituents: head group, chain or backbone, and the tail group (Fig.2.3).

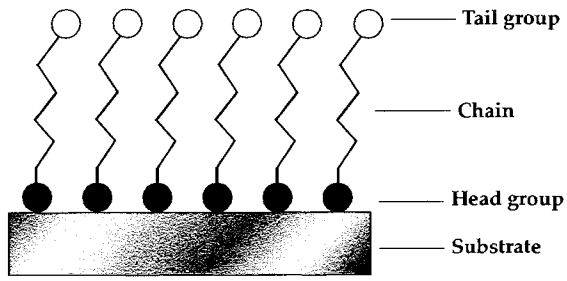

Figure 2.3: Schematic drawing of the SAM molecule constituents. The shaded circle represents the head group that is chemisorbed onto the substrate. The end group is indicated by the open circle and it can be a variety of chemical functional groups.

Recently, applications and the characteristics of SAMs have been extensively studied by researchers in a wide spectrum of fields. The reason SAMs have become so attractive is the SAM head groups can preferentially bind to defined areas of the substrate and the tail groups can be substituted to further tune the surface chemistry of the film for any specific

application. This also means that specific functional groups can be selectively modified while leaving the rest of the molecules unchanged. For example, the surface of alkylsilane (Cl_3Si–R, where R can be any alkyl group) monolayer can be switched from hydrophobic to hydrophilic by simply changing the tail group from a hydrocarbon (*e.g.*,–CH_3) to hydroxyl (–OH). These special characteristics of SAM molecules have been exploited in many applications such as microcontact printing [74–76] and nanolithography [77, 78]. Generally, SAM systems are defined by the chemisorbing head group and the substrate, and these systems can be prepared through either solution or vapour-phase surface treatment methods. One of the most commonly studied SAM systems is the attachment of thiols (–SH) on gold surfaces. Due to the inertness of the gold substrate and the well-defined order of the thiol molecules, the *n*-alkanethiol on gold system has become the model system for SAMs formed on all other substrates. Siloxane-based SAM systems and their surface chemistry also have been well-established for controlling the surface properites of various substrates (*e.g.*, glass, indium tin oxide coated glass). The versatility, durability and applications of SAM systems are well illustrated by works using these molecular films in the ordering of metal nanoparticles [79], improving the performance of organic optoelectronic devices [57, 61, 80, 81] and enhancing the adhesiveness of chemical vapor deposited (CVD) copper layers [82]. The low costs and ease of preparation of SAMs make them the ideal method for surface functionalisation.

Prior to SAM fabrication, the substrates used for deposition need to be properly cleaned. Crystalline metal substrates are the most commonly used substrates for SAM deposition. The classical method for cleaning these metal surfaces is ion sputtering and annealing. However, a piranha solution (1:3 volume % mixture of concentrated H_2SO_4 and H_2O_2) [83] is usually used for the cleaning of silicon substrates. Silicon substrates are the most common substrates used for silane-based SAMs because silicon has a native oxide layer that can be utilised for bonding with the silicon head group of a silane-based molecule. Generally, the choice of substrates depend solely on the molecules to be deposited.

Solution deposition of SAM

The principle of solution deposition of SAMs is straightforward. A clean substrate is dipped or immersed into the corresponding organic solution and allowed to react for a certain amount of time (Fig. 2.4). During the process, a monolayer of molecules will assemble onto the substrates without intervention [83]. Following the assembly of the monolayer, the substrate must be rinsed thoroughly according to an appropriate procedure to ensure the byproducts of the reaction are completely removed. Finally, the films may be annealed in air to further dissociate any byproducts, particles, or organic moieties that are not bonded to the substrate surface. Repetition of this solution deposition procedure results in multilayered films, depending on the organic molecule employed [57]. The quality of the SAM depends heavily on the cleanliness of the solution. For example, water content is detrimental to the preparation of SAMs for silane-based systems because many silane molecules will react with water molecules, and hence are water sensitive. In such case, the solution must be properly outgassed and the reaction must be executed under a dry atmosphere (*e.g.*, nitrogen, argon).

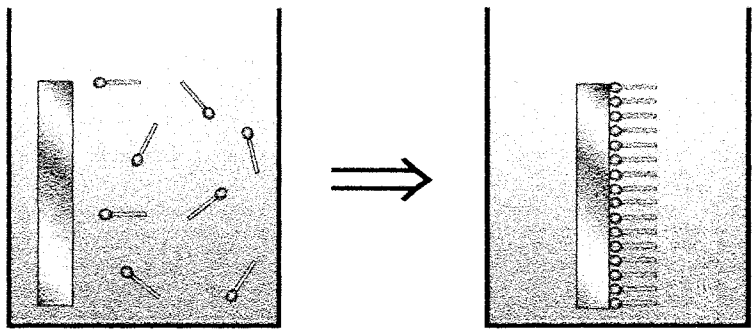

Figure 2.4: Schematic drawing of the solution deposited monolayer. A monolayer of molecules self-assembled onto the substrate when the substrate is fully immersed into the solution.

Vapour-phase deposition of SAM

The less popular method for the preparation of SAMs is vapour-phase deposition and this can be done using a few different techniques. Traditionally, gas phase deposition of SAMs occurs in a ultrahigh vacuum (UHV) chamber of a surface science tool (*e.g.*, the chamber

of a scanning tunneling microscopy (STM) instrument) [84–86], similar to OMBE. Inside such a chamber, only one additional port is needed to attach a valve and a dosing line, through which the molecules can be released in the manner of a controlled molecular flux (Fig. 2.5) [87]. Most surface science tool chambers allow the substrate to be cleaned via ion sputtering and annealing prior to deposition. Hence, the substrates are kept extremely clean throughout the deposition process and ultrahigh purity films can be produced using this method. Yet, this method of vapour-phase deposition of SAMs is more expensive as compared to solution deposition; consequently, it has only been employed when *in-situ* characterisation of SAMs during deposition was desired. The advantage of UHV systems are the extremely clean deposition environment and the ability to precisely control the layer thickness.

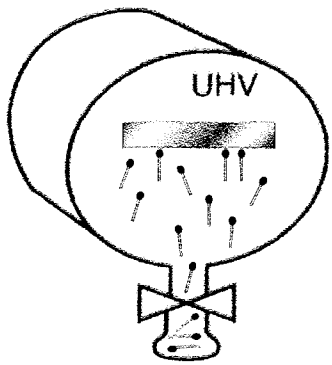

Figure 2.5: A schematic drawing of vapour-phase deposition of SAM in an ultrahigh vacuum (UHV) chamber.

Vapour-deposition of SAMs can also be done in a chemical vapour deposition (CVD) system [88]. In a simple CVD chamber, the substrate is placed on a heated holder with the molecules or reactant inlet positioned above the substrate. A controlled flow of vapour phase molecules enter the reaction chamber through the inlet and assembles onto the substrate surface to form an organic layer. The substrate is usually heated to ensure activation of the chemical reaction between the substrate and the molecular flux at the substrate surface. Then the byproducts of the reaction are pumped out by an exhaust outlet placed underneath the substrate (Fig. 2.6).

A more common gas deposition technique for SAMs utilises a reactor vessel similar to

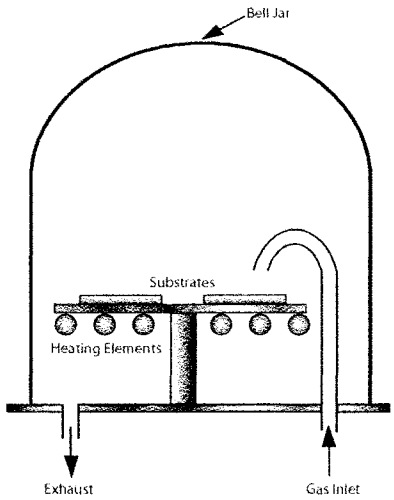

Figure 2.6: Schematic drawing of a simple chemical vapour deposition system (CVD) used in the fabrication of SAMs.

a vacuum desiccator (Fig. 2.7). This technique is very similar to CVD, but less expensive and much easier to prepare. Here, the clean substrates are simply placed inside the vacuum desiccator with a open glass vial containing few drops of the organic solution. The organic molecules will naturally evaporate with time and self-assemble onto the substrate surface [83, 89]. Both vacuum and heat may be applied to the desiccator or reaction chamber to increase the reaction and vaporisation rate. It is worth noting that some molecules cannot be used in this type of vapour-phase deposition because the byproducts may re-attach to or react with the substrate due to the lack of exhaust pump for waste products in this system.

2.3 Applications of Organic Thin Films to GLAD

The various types of organic thin film types mentioned above can be used to control the interactions of materials with their environmental surroundings, which is of extreme importance in many applications such as chemical sensors and optical devices. For example, humidity sensors require high sensitivity towards water vapour in the atmosphere while still being very selective to minimize false positive responses. One important factor that can be readily controlled through geometry and tailored surface chemistry via organic thin films is wettability. The wettability of a fluid on a substrate is dependent on the similarity of surface energies of that fluid and the substrate. The more alike the surface

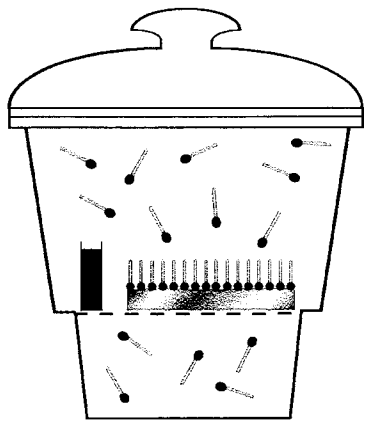

Figure 2.7: Schematic drawing of vapour-phase deposition of SAM inside a desiccator. Molecules vapourised from the small glass vial will self-assembled onto the substrate.

energies are, the more adhesive the desire fluid will be to the surface of the substrate. However, since many chemical properties (*e.g.*, polarity) are measured with respect to water, it is not surprising that in most cases, wettability also refers to the substrate's affinity for water. Hence, the wettability of most materials can be defined as either hydrophilic or hydrophobic. A surface is considered hydrophobic if it is insoluble in water and will not adsorb water. In contrast, a hydrophilic surface has a strong affinity for water and is soluble in water. Generally, there are two ways to increase surface hydrophobicity: (1) increasing substrate surface area of hydrophobic materials and (2) modifying rough surfaces to lower the surface energy. Recently, there has been much interest in the creation of superhydrophobic materials arising from the "self-cleaning" ability of these materials, as well as the wide range of possible applications including automobile windshield coatings, paint and interior fabric coatings. Nanostructures such as aligned carbon nanotubes [90,91], ZnO nanorods [92], and dendritic gold nanoclusters [93] all exhibit superhydrophobicity and may be classified into category 1. Other groups have demonstrated the realization of superhydrophobic surfaces via the second approach, and examples of these include lowering the surface energy of Cu and conductive ZnO film through chemical treatment and self-assembly [91]. Unfortunately, high surface area nanostructures of tailored surface chemistry either lack order in the underlying nanostructures (*e.g.*, porous silica) [94] or have been prepared by inconvenient and costly methods such as plasma deposition [95].

Glancing-angle deposition provides porous, high surface area, nanostructured thin films that can be sculpted into a variety of structural motifs. These properties of GLAD films make them well suited for applications such as chemical sensing and catalysis, antireflection coatings, and photonic crystals. In the following chapters, the first application of chemical functionalization to tailor the surface energy of complex, porous GLAD films and its applications in chemical sensing and optical devices will be described.

3

Experimental Design and Methods

This chapter describes the experimental procedures and methods used in the deposition and surface functionalisation of glancing angle deposition thin films. In particular, the fabrication and chemical treatment of the three specific types of GLAD structures (slanted posts, vertical posts and helices) are given in detail. Various alkyltrichlorosilane and methoxysilane reagents are used to functionalise the GLAD films to achieve varying degrees of hydrophilicity or hydrophobicity. It is still an open question whether the surface functionalisation techniques described here can be called self-assembly because the degree of order in the organic layers formed on the surface of the GLAD structures has not been investigated. Furthermore, the thickness of the organic layer has not been measured, and thus cannot be definitively described as a self-assembled monolayer. However, similar principles and methods utilised in the preparation of SAMs were employed here in the surface functionalisation of GLAD films.

3.1 Glancing Angle Deposition

The GLAD films employed in this thesis have been deposited on a variety of substrates including Si{100}, borofloat glass, indium tin oxide-coated borofloat glass (ITO), and

quartz. Many substrates were chosen for the ease of characterisation and functionalisation. For example, silicon wafers were used in every deposition since they are straightforward to cleave into appropriate sizes for scanning electron microscopy (SEM) imaging. Quartz substrates are ideal for IR spectroscopy analysis because of the high cutoff wavelength for the transmission spectra. Various other substrates were chosen for much of the same reasoning.

Prior to glancing angle deposition, the silicon wafers, supplied by Evergreen Semiconductor Materials, were cleaned by immersing them in piranha solution (1:3 vol. % mixture of concentrated H_2O_2:H_2SO_4) for approximately 30 minutes. The substrates were subsequently rinsed with de-ionized water and dried under nitrogen atmosphere. ITO coated glass, blank borofloat glass, and quartz substrates supplied by Precision Glass & Optics were used as received. Any small particles and dust on the substrates were blown off using a stream of nitrogen gas before thin film deposition.

Three basic GLAD structures, slanted posts, vertical posts and helices, were fabricated using the glancing angle deposition system. Evaporant source material (SiO_2, TiO_2, and Al_2O_3) were obtained as 99% purity 3-6 mm pieces and used as received from CERAC Inc. The various types of GLAD structures were fabricated with evaporant material mentioned above using two different electron-beam evaporation systems. One of the systems was a Kurt J. Lesker AXXIS (Fig. 3.1) and the other was a system supplied by CHA Industries (Fig. 3.2). For the Kurt J. Lesker AXXIS, a software program, accompanying the evaporation system, is used to control the substrate position and motions, as well as the pump down procedure. On the other hand, a LabVIEW software program was developed by fellow group members [96–98] for the CHA Industries system to control the substrate position and motions.

In both cases, a crystal oscillator thickness monitor (CTM) continuously feeds the current deposition rate and film thickness into a computer system. The computer system in turn sends instructions to the stepper motors, and thus controlling the polar and azimuthal position of the substrate. However, the motor control in the AXXIS system is slightly more precise than the CHA system since the user can manually define both speed and position of the motor through the software program. Also, the emitter in the AXXIS system can

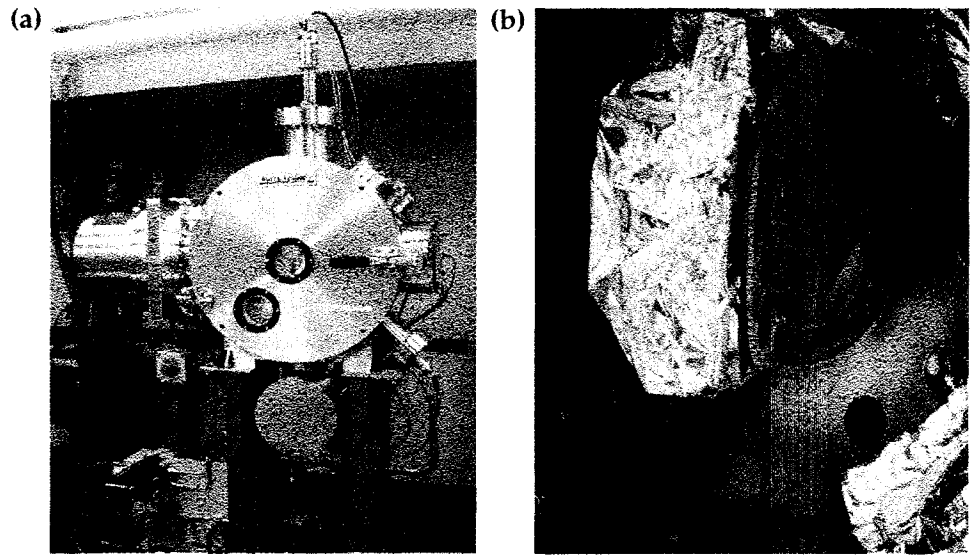

Figure 3.1: Images of the Kurt J. Lesker AXXIS evaporation system: a) exterior of the vacuum chamber, and b) the interior of the vacuum chamber containing the CTM and substrates on the chuck.

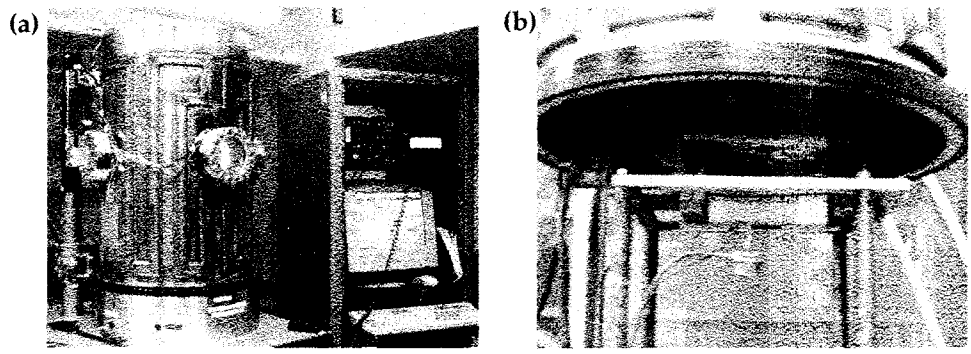

Figure 3.2: Images of the CHA Industries evaporation system: a) exterior of the vacuum chamber along with electronic control panel and b) the interior of the vacuum chamber containing the CTM and the chuck.

focus the electron beam much better than the old CHA system, as well as having more accurate control over the position of the scanning electron beam. By combining the more focused electron-beam with the more precise position and motor control, the uniformity and the fineness of the structures are greatly improved. However, both systems have an extra inlet where a stream of oxygen gas can be added to the chamber to prevent the depletion of oxygen gas during deposition of an oxide film. The geometric source to substrate separation length is 40 cm in both systems. There is a slight difference in the location of the CTM

between the two systems, which implies the geometric factor that relates the deposition rate and film thickness at the CTM to the actual deposition rate and film thickness at the substrate is different from system to system. For the project at hand, the structure of the film and the uniformity is not of essential importance, and will not affect processing of the films and/or results from the surface functionalisation of GLAD films. However, for consistency, only films grown in the same system were compared with each other.

In general, the base pressure and deposition pressure varies with the evaporant material and is dependent on the ability of the pumps in the system to achieve low pressure. Tables 3.1 and 3.2 details the base pressure and operating chamber pressure used in the deposition of three different metal oxides on the CHA and AXXIS systems, respectively. TiO_2, SiO_2, and Al_2O_3 GLAD films of slanted, vertical and helical columnar structure were fabricated by electron-beam evaporation using a modified literature procedure [99, 100]. Typical electron-beam acceleration voltage values ranged from 8.0 to 9.0 kV with approximate current values of 40 mA, 200 mA, and 150 mA for SiO_2, TiO_2, and Al_2O_3, respectively. The electron-beam was then programmed to sweep in a figure-8 pattern over the material throughout the deposition. 6 MHz alloy crystal supplied by Phelps Electronics, Inc. were used in the crystal thickness monitor (CTM) to track *in-situ* film thickness and deposition rate. Each metal oxide was placed in an 8.2 cm^3 carbon crucible supplied by POCO Graphite and deposited onto a variety of substrates including: Si wafer, ITO-coated glass, and borofloat glass at $\alpha = 85°$. To obtain a 2.0 μm slanted post film, the substrate was maintained at $\alpha = 85°$ with no rotation about the axis normal to the substrate (ϕ). Uniform helical structures formed when the substrate was held at $\alpha = 85°$ while rotating at 0.21 rpm about the ϕ axis with the CTM deposition rate was maintained at 14 Å/s. The vertical post morphology was fabricated by holding the substrate constant at $\alpha = 85°$, and rotating the substrate at a much faster rate of $\sim$17 rpm about the ϕ axis while maintaining the CTM deposition rate at 18 Å/s.

3.2 Reactive Ion Etching

Prior to surface functionalisation, all film samples were treated with a short oxygen plasma reactive ion etch (RIE). Oxygen plasma RIE is a well known technique for saturating oxide

Material	*Base Pressure* (Torr)	*Deposition Pressure* (Torr)
SiO_2	$<5\times10^{-6}$	$<8\times10^{-4}$
TiO_2	$<8\times10^{-7}$	$<5\times10^{-5}$
Al_2O_3	$<4\times10^{-7}$	$<2\times10^{-5}$

Table 3.1: The pressure used for the deposition of GLAD films varying with the type of material and the ability of the system.

Material	*Base Pressure* (Torr)	*Deposition Pressure* (Torr)
SiO_2	$<6\times10^{-7}$	$<2\times10^{-5}$
TiO_2	$<2\times10^{-7}$	$<5\times10^{-5}$
Al_2O_3	$<2\times10^{-7}$	$<3\times10^{-5}$

Table 3.2: The pressure used for the deposition of GLAD films varying with the type of material and the ability of the system.

surfaces with reactive, hydrophilic hydroxyl (–OH) groups. [61] When the substrate surface is bombarded with oxygen ions, it becomes saturated with O_2 sites. Upon exposure to air, hydroxyl groups are formed on the substrate surface through chemisorption of water vapour in the atmosphere. This process is essential for surface functionalisation with siloxane-based chemistry because silane functionalities have high reactivity towards hydroxylated surfaces. Thus, saturating the surface with hydroxyl moieties maximises the reactivity between the metal oxide GLAD pillars and the alkyltrichlorosilane reagents.

It is important to note that since the oxygen plasma RIE process is generally used for etching of materials, the GLAD pillars will be etched away if the RIE process were applied for too long. Hence, a balance between saturating the surface with hydroxyl moieties and not affecting the GLAD structures during the RIE exposure is essential. The effect of different lengths of RIE exposure time was examined to find the time that would produce the best balance between hydroxyl saturation and etching of the GLAD films.

RIE treatment of the GLAD films was performed on a Plasmalab RIE 80. Fourier Transform Infrared spectrometry (FTIR) was used to identify the amount of the -OH and moieties on the surface of GLAD pillars before and after RIE treatment. FTIR is a quick and relatively inexpensive spectroscopic technique that is useful for identifying chemical functional groups within a molecule (*e.g.*, –OH groups, double bonds, single bonds, –CH groups, etc.) [101]. In IR spectroscopy, the infrared radiation induces vibrations in a molecule. Each type of vibration can be in turn associated with the motions of a functional

Bond	Wavenumber (cm^{-1})	Wavelength (nm)
C–H	3000 - 2850	3333 - 3510
=C–H	3100 - 3000	3226 - 3333
≡C-H	3300	3030
O=C–H	2800 and 2700	3570 and 3700
O–H	3600 - 3000	2778 - 3333
N–H	3450 - 3100	2900 - 3226

Table 3.3: The position of vibration bands for functional groups with single bonds to hydrogen is described in this table.

group in that molecule. It is these motions or vibrations of the molecule that are measured in IR spectroscopy, and the different functional groups are identified by the position and/or pattern of absorption/transmission/reflection bands or peaks. Generally, interpretation of IR spectra data is done by referring to charts and tables of infrared data. There are many tables available for reference, and the data that is relevant to this project is given in Table 3.3 [102].

The series of FTIR studies were performed on a Nicolet Magna 750 FTIR instrument with a broadband infrared source supplied by Ever-Glo (TM). FTIR spectra were obtained using 32 scans with a mercury cadmium telluride (MCT-B) detector and a resolution of 4 wavenumbers. Data acquisition was performed using the supplied proprietary Nicolet Omnic software. Happ-Genzel apodization, Mertz phase correction, and manual base-line correction were performed on the collected data. In the data collection process, the IR beam first passes through a reference substrate, which is a blank substrate made of the same material as the substrate the actual sample is on, and the instrument records the intensity of the transmission across a range of wavenumbers. Subsequently, the reference substrate is replaced with the actual sample and the resulting graph compares the difference in intensity between the transmission plots produced by the actual sample and the reference substrate. For easy interpretation, the wavenumbers have been converted to wavelength for all FTIR spectra presented in this thesis using equation 3.1.

$$Wavelength\ (\lambda) = \frac{1}{Wavenumber}\ [cm] \tag{3.1}$$

Note that the units for wavenumber is in cm^{-1}; hence, the units for calculated wavelength

is in centimetres instead of metres.

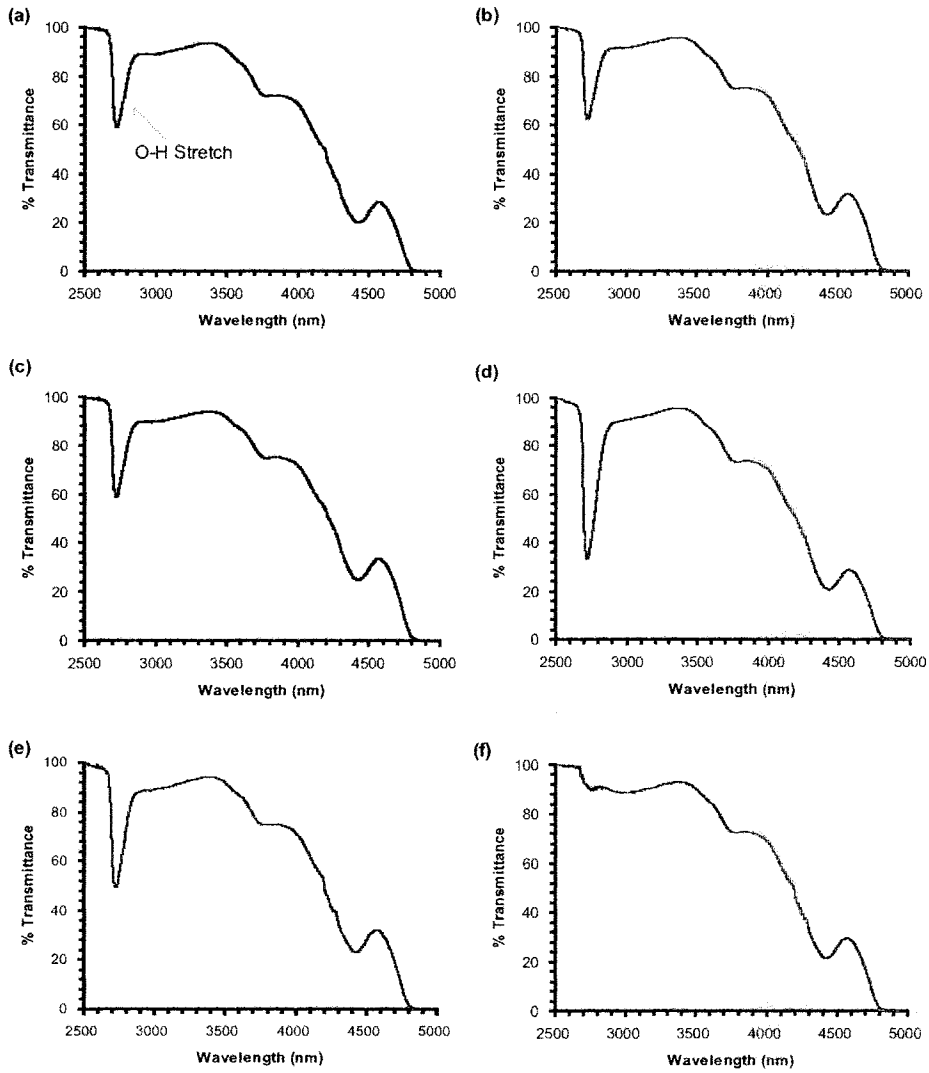

Figure 3.3: Infrared spectra of SiO_2 GLAD film with a) no RIE treatment, b) 30 s, c) 60 s, d) 90 s, e) 120 s and f) 150 s of O_2 plasma RIE exposure.

The IR spectra of a helical structured GLAD films with RIE exposure time ranging from 30 to 150 seconds is given in Fig. 3.3. For this study, multiple samples of the same film on quartz substrates were used. A blank quartz substrate is used as the reference substrate, and its transmission spectrum is subtracted from spectra of the film samples. To analyze the IR spectra, the author referred to the IR data table given above (Table 3.3) to identify the type of functional groups on the surface of the film. Since the purpose of the short RIE exposure is to saturate the film surface with hydroxyl groups, the presence and intensity of the O–

H stretch in the IR spectra of the film determines the effectiveness of RIE treatment for increasing the density of –OH groups on the film surface. From the IR spectrum of GLAD films with a RIE exposure of 0-120 s (Fig. 3.3a - e), a large decrease in % transmittance is noted at the wavelength of ~2800 nm, which corresponds to the position of free hydroxyl groups. Furthermore, the intensity of the dip in the spectrum varies with the length of time of RIE exposure. This suggests that RIE treatment effectively changes the density of –OH groups on the film surface and confirms the fact that hydroxyl groups are in fact present on the film surface. According to the FTIR spectra, the intensity of the O–H stretch appears to be the greatest at 90 s of RIE exposure time (Fig. 3.3d), and decreases as the exposure time increased past 90 s. In fact, at 150 s of RIE exposure time, the O–H stretch is not present at all, which suggests that the oxygen plasma has started to etch the oxygen moieties in the SiO_2 film. Hence, by exposing the GLAD films to 90 s of RIE treatment, a maximum density of surface hydroxyl groups is achieved without deteriorating the structure or etching the surface of the film. Micrographs of the film before and after the various times of RIE treatment, taken using a scanning electron microscopy (SEM) instrument, confirmed that there was no deterioration in the structure of the film arising from the RIE exposure for the times tested.

3.3 Surface Functionalisation

Two methods of surface functionalisation, solution and vapour-phase, were used to tailor the surface properties of various materials. The concept behind both methods of functionalisation is similar to the self-assembly technique which utilises the reactivity of the hydroxyl groups with chlorosilyl functionalities to covalently bond organosilane molecules onto the surface of GLAD pillars. In brief, the Si head group of alkyltrichlorosilane or methoxysilane molecules have a preferential affinity for hydroxyl groups, and thus will attach themselves to the –OH groups once they come into contact with the hydroxylated film surface. The order of these self-assembled molecules and the thickness of this organic layer have not been investigated since both order of the molecules and thickness of the organic film would not affect the results of this research project. However, because the thickness and the order of the organic molecules was

not examined, the organic film cannot conclusively be referred to as a self-assembled monolayer. Nevertheless, the two functionalisation methods untilises the general concepts of self-assembly described in Chapter 2 to tailor the surface chemistry of metal oxide GLAD films.

3.3.1 Solution-based functionalisation of GLAD films

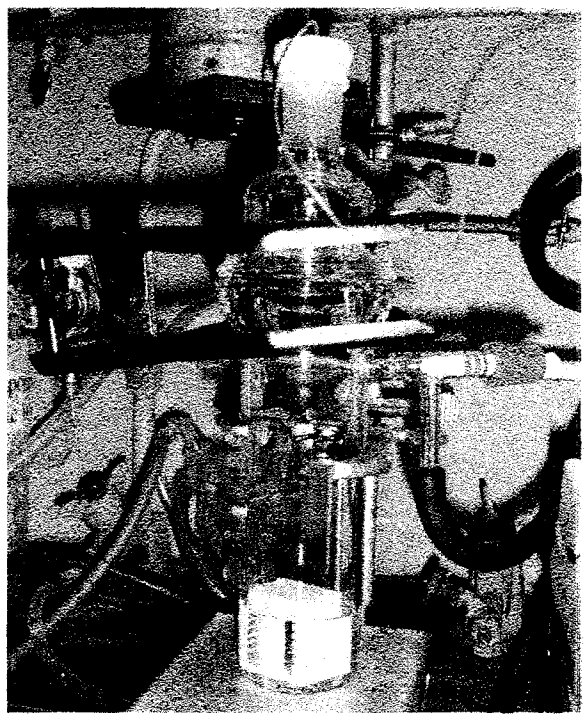

Figure 3.4: An image of substrates undergoing siloxane-based solution reaction in a glass reaction vessel.

Substrates were placed in an inert teflon holder inside a dry, clean glass reaction vessel (Fig. 3.4), which was connected to the Schlenk line. Subsequently, the vessel was flushed with nitrogen gas and then purged by applying a vacuum according to strict Schlenk protocol. This flushing/purging process was repeated 3× or until there was no more air inside the glass vessel. Using a canula, a stream of dry, de-oxygenated 20 mM toluene (supplied by Fisher Scientific) organosilane solution (vinyl-trichlorosilane, octadecyl-trichlorosilane, 3,3,3-trifluoropropyl-trichlorosilane, or 7-octen-1-yl-trimethoxysilane supplied by Aldrich Chemical Co.) was expended into the vessel until the substrates were completely submerged in solution and allowed to react for 24 hours

under nitrogen atmosphere. Once the reaction was completed, the solution was removed using a canula and the samples were rinsed three times with dry toluene under nitrogen atmosphere. Finally, the samples were immersed in 0.5% H_2O acetone (supplied by Fisher Scientific) to hydrolyze any residual Si–Cl functionalities and annealed in air for 24 hours at 165°. This solution derivatization method was used to functionalise substrates (Si {100}, glass, ITO, and quartz) with and without metal oxide GLAD films (SiO_2, TiO_2, and Al_2O_3). Three basic GLAD structures (slanted post, vertical post, and helices) were fabricated using SiO_2 evaporant, and these structures were derivatized with vinyl-trichlorosilane using the solution method as described above. This allows the examination of structural effects, if any, on the wettability of surface functionalised GLAD films. Once the structural effects are observed, only helical structures of silica, alumina, and titania GLAD films were compared in the functionalisation studies.

3.3.2 Vapour-phase functionalisation

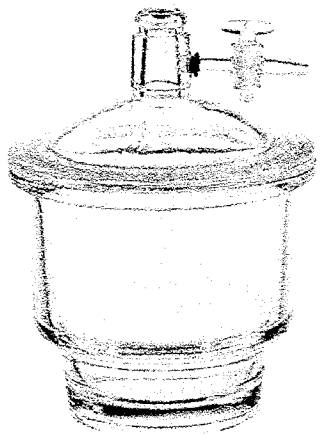

Figure 3.5: An image of the glass vacuum desiccator used in present studies.

The procedure for vapour-phase functionalisation was much simpler than functionalisation using solvents. 1.0 mL of organotrichlorosilane (vinyl-trichlorosilane, 3,3,3-trifluoropropyl-trichlorosilane, octadecyl-trichlorosilane) or organotrimethoxysilane (7-

octen-1-yl-trimethoxysilane) solution was transferred, as-received, into a glass vial using a syringe. The glass vial was then placed into a vacuum desiccator (Fig. 3.5). Next, the film samples were placed in the vacuum desiccator along with the glass vial containing the organosilane reactant. The substrates were allowed to react for 48 hours under reduced static pressure in an atmosphere saturated with the organosilane reagent. However, only three types of organosilane solutions were tried here because it was expected that all other silane-based solutions would function in much the same way as the three trial solutions; however, this matter was not pursued further.

4

Tailoring the Surface Chemistry of GLAD Films Through Siloxane-based Surface Chemistry

Siloxane-based surface chemistry is a well-established method for controlling the surface properties of a wide variety of substrates (*e.g.*, glass, indium tin oxide-coated glass, porous silica). The versatility and durability of siloxane-tethered molecular films are well illustrated by works using these robust surface moieties in nanolithography [77, 78, 103, 104], ordering colloidal gold nanoparticles on substrates [105], microcontact printing [74–76] and enhancing the performance of organic light-emitting diodes [20, 61, 106]. Siloxane-based surface chemistry (Scheme 4.1) is an ideal method for introducing a chemical "dimension" to the tunability of GLAD films since it offers the possibility of chemical reactivity as well as extreme hydrophobicity using commercially available reagents. This chapter describe the first application of siloxane-based surface chemistry to complex, three-dimensional SiO_2 GLAD films and the formation of superhydrophobic silica surfaces. The superhydrophobicity of the GLAD films is a result of the synergistic effects of the film dimension and tailored surface chemistry. Here, SiO_2 GLAD films of slanted, vertical, and helical post structures on Si{100} and ITO substrates were

solution functionalized with vinyl-trichlorosilane, octadecyl-trichlorosilane and 3,3,3-trifluoropropyl-trichlorosilane. Si{100} and ITO substrates with and without GLAD films and/or chemical functionalization were characterized with scanning electron microscopy (SEM), x-ray photoelectron spectroscopy (XPS), advancing aqueous contact angle measurements. GLAD films on ITO-coated substrates were also evaluated with cyclic voltammetry to investigate whether the functionalisation effectively penetrated the entire film.

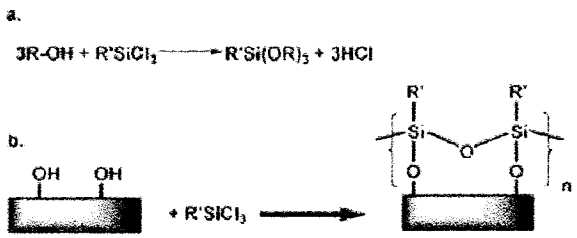

Figure 4.1: A schematic of alkyl trichlorosilane reaction with hydroxylated substrate surface.

4.1 Scanning Electron Microscopy(SEM)

Scanning electron microscopy images of representative pre- and post-functionalised SiO_2 films were taken using a JEOL6301F field-emission scanning electron microscope with an acceleration voltage of 5 kV. These images are presented in Figure 4.2. The SEM images confirm that no deterioration in the SiO_2 structure arises from short RIE exposure and the GLAD films stay intact throughout the surface derivatization procedure.

4.2 X-ray photoelectron spectroscopy (XPS)

XPS is an analytical technique for establishing the composition of the outer few atomic layers at the surface of a material. This technique has been extensively studied and employed as a surface characterisation method by many researchers [107, 108] because it can detect all the elements to a sensitivity in the range of 0.1-1%, except for hydrogen and helium, which are too light in weight to be detectable by the XPS system. A monochromatic beam of x-rays is used as the radiation source in XPS. When the source x-ray photons strike

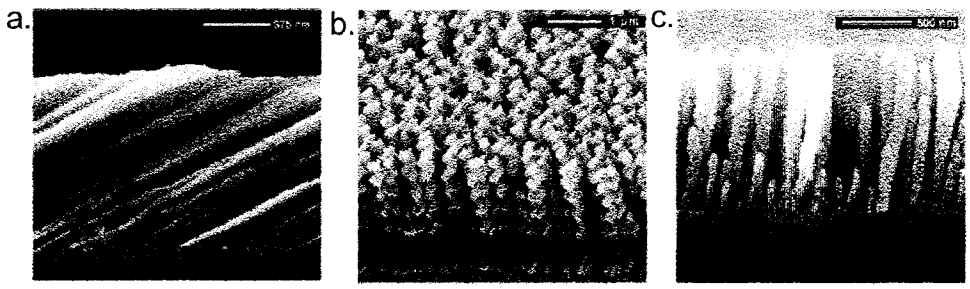

Figure 4.2: Representative SEM images of functionalised and unfunctionalised SiO_2 nanostructures grown by glancing-angle deposition: (a) slanted posts, (b) helical columnar pillars, and (c)vertical posts.

the surface atoms at ground state core energy level E_x, characteristic x-ray photoelectrons are ejected directly from the atom at E_x. The XPS instrument then detects the binding energy (E_p) of the ejected photoelectrons according to the following equation [108]:

$$E_p = h\upsilon + E_x - \Delta_p \tag{4.1}$$

Where $h\upsilon$ is the source x-ray photon energy, E_x is the ground state core energy, and Δ_p is the chemical shift term, which is dependent on the chemical binding state of the atom. Subsequently, the mass percentage of the elements on the surface of a material is determined by the peak intensities of the ejected photoelectrons at specific binding energies. Thus, the emitted XPS spectra contain information on the chemical state of the surface atoms, and the composition as well as the mass percentage of the atoms on the surface of a material. Composition of layers below the surface can also be studied using a depth profile operation mode, where the surface atomic layers are sputtered away using an *in situ* argon ion beam in the energy range of 0.5-5 keV. The damaging effect of the XPS source radiation is usually very weak and charging effects are minimal; hence, both organic and insulating materials can be easily studied with almost no noticeable effects. In the present studies, all XPS spectra were obtained using a Kratos Axis Ultra instrument operating in energy spectrum mode at 210 W. The base pressure and operating chamber pressure were maintained at $\leq 10^{-9}$ Torr. A monochromatic Al Kα source was used to irradiate the samples and the spectra were obtained with an electron take-off angle of 90°. The wide survey spectra were collected using an elliptical spot with 2 mm and 1 mm major and

minor axis lengths, respectively, and 160 eV passing energy with a step of 0.33 eV. Film compositions were determined from the peaks of the survey spectra with subtracted linear background using the internal instrument values of relative sensitivity factor.

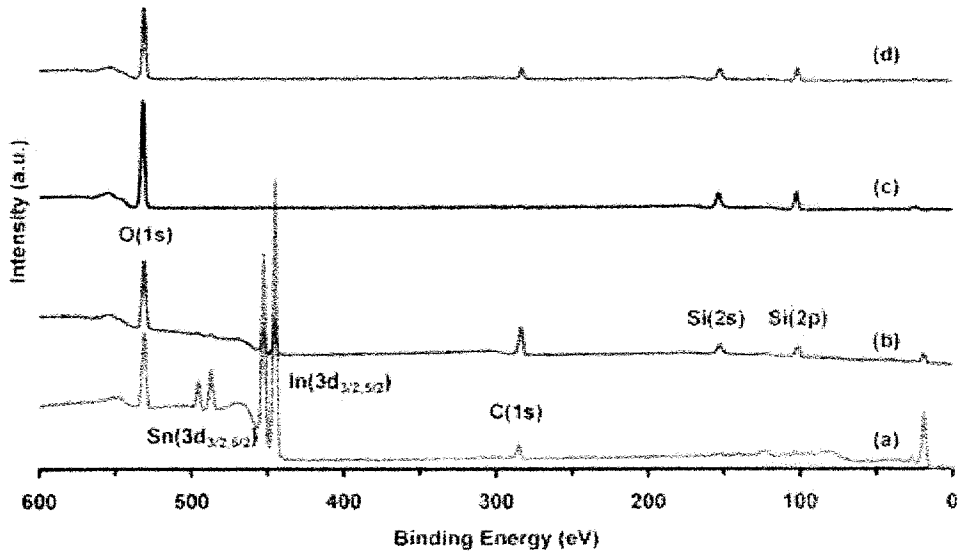

Figure 4.3: X-ray photoelectron spectroscopy of (a) the bare ITO-coated glass substrate, (b) vinylsiloxane-derivatized ITO glass, (c) untreated helical SiO_2 GLAD film on ITO glass, and (d) vinylsiloxane-derivatized helical SiO_2 GLAD film on ITO glass. This spectra is modified from [109].

XPS spectra of blank ITO and GLAD films on ITO provides insight into the effect of chemical derivatization procedure. XPS analysis of unmodified ITO substrates show characteristic Sn(3d) and In(3d) emissions (Fig. 4.3a). The C(1s) emission noted in the bare ITO substrate can be ascribed to adventitious carbon in the ITO. Upon surface functionalization with vinyl-trichlorosilane, concomitant decreases in the Sn(3d) and In(3d), increase in the C(1s), and appearance of the Si(2s) and Si(2p) emissions (Fig. 4.3b) are observed. The noticeable increase in C(1s) emission for alkyl-derivatized substrates (with and without GLAD film) was doubtless the result of a combination of the adventitious carbon and the overlying surface functionality. XPS analyses of all SiO_2 GLAD films on ITO, independent of film morphology, show no characteristic photoemission from the underlying ITO substrate (Fig. 4.3c). The GLAD film thickness ($\sim$2 μm) appears to mask the signature ITO emissions given that XPS analysis surveys depths of sample ranging

from 5-100 Å. This masking of the adventitious C(1s) signal from ITO substrate allows a direct comparison of the C(1s) emission from functionalised and unfunctionalised GLAD films (Fig. 4.3c and 4.3d). Both the presence and absence of the C(1s) emission in the functionalised and unfunctionalised GLAD film, respectively, confirms the attachment of organic surface moieties, and thus a change in the surface chemistry of the SiO_2 pillars. It is important to note the absence of the Cl(2p) photoemission peaks in all the spectra of alkyl-derivatized substrates, indicating full hydrolysis of the Si–Cl bond and the effective removal of the HCl byproducts in funcctionalisation procedure. Similar results have been noted for Si{100} substrates.

4.3 Advancing aqueous contact angle measurements

Contact angles are generally used for measuring the surface energy of a material and it is attractive because it provides a easy way for estimating the solid-vapor and solid-liquid interfacial tensions. The equilibrium relationship between the contact angle ($\theta*$) of a liquid drop on a uniform solid surface and the solid surface tensions, solid-vapour (γ_{sv}), solid-liquid(γ_{sl}), and liquid-vapour(γ_{lv}), is defined by Young's equation [110]:

$$\gamma_{lv} \cos \theta^* = \gamma_{sv} - \gamma_{sl} \tag{4.2}$$

The contact angle refers to the angle of a tangent line drawn from the base of a liquid drop that is in contact with a solid substrate (Fig. 4.4). To measure the contact angle, a drop of liquid is formed at the end of a syringe and this drop is carefully placed on the substrate surface. For advancing contact angle measurements, the syringe can be retracted after the placement of the drop on the substrate surface. The advancing contact angle is measured when the liquid is fully expanded on the surface (*i.e.*, the measurement is made soon after the drop contacts the substrate surface). However, in receding angle measurements, the syringe is kept inside the drop of liquid, without deforming the shape, while the liquid is extracted. Hence, the receding angle is measured when removal of any more liquid from the drop will cause contraction of the interfacial area. Generally, the advancing contact angle is the "wetting angle" and it is the largest possible angle because any further increase

of drop volume will cause the drop to expand and ready to "wet" additional liquid-solid interfacial area. In contrast, the receding angle is the smallest possible angle, and also is referred to as the "de-wetting angle".

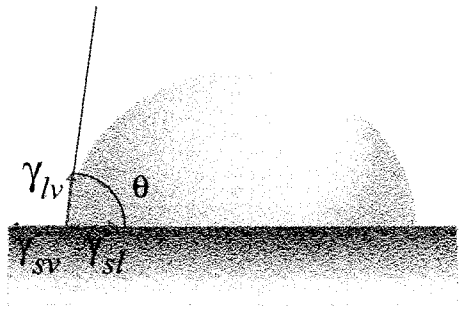

Figure 4.4: A schematic of the contact angle of a liquid on a solid surface.

However, there is always a difference between the contact angle made by an advancing liquid (θ_a) and a receding liquid (θ_r) on a solid surface, and this difference is known as the contact angle hysteresis (H):

$$H = \theta_a - \theta_r \tag{4.3}$$

Contact angle hysteresis is primarily due to surface roughness and/or chemical heterogeneity of the solid surface. Nearly all solid surface exhibit contact angle hysteresis because no surface is completely smooth at the microscale. It has been experimentally found that contact angles tend to be larger on rough surfaces than on chemically identical smooth surfaces [111]. Young's equation cannot be used to predict the contact angles on rough surfaces because the fact that contact angle measurements on very rough surfaces inevitably reflect surface topography rather than surface energy alone. Unfortunately, Young's equation only accounts for surface tension (or surface energy), and not topography. Hence, contact angles and surface tensions predicted by Young's equation are only accurate for smooth solid surfaces that are chemically uniform. However, Young's equations still provides a good approximation of interfacial surface tensions for smooth heterogeneous surfaces if advancing contact angle is used. In the case of a rough solid surface, the surface area of the material will increase due to the presence of the surface microtexture, and the

drop of probing liquid can behave in two ways. In the first case, the liquid follows the solid surface, that is, it fills the voids of the microstructures on the material's surface, and the liquid may spread depending on the hydrophilicity or hydrophobicity of the surface (Fig. 4.5a). The other case is that there is minimal contact between the drop of liquid and the top of the microstructure resulting from air trapped inside the microstructure or trough (Fig. 4.5b).

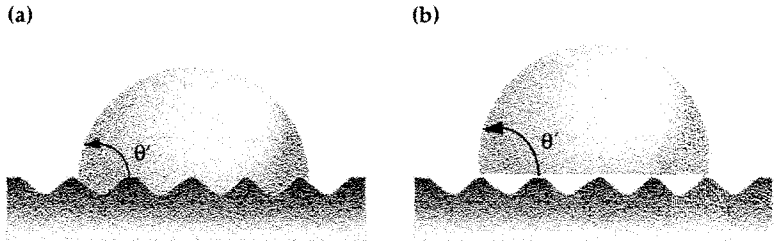

Figure 4.5: The two states of liquid behaviour on rough surfaces: a)the Wenzel state where liquid fills in the voids of the microstructure, and b) the Cassie and Baxter state where air is trapped between the liquid and solid substrate interface.

Wenzel [112] proposed a theoretical model for contact angles on a rough surface, where the drop of liquid follows the behavior described in the first case:

$$\cos\ \theta' = r \cos\ \theta^* \tag{4.4}$$

where θ' is the apparent contact angle on the rough surface, r is the surface roughness factor and θ^* is the intrinsic contact angle on a flat surface. The surface roughness factor is defined as the ratio between the true surface area and the geometric projected area. This surface roughness factor r is a number always larger than unity because regardless of the surface's affinity for water, the wetting properties of the surface will always be magnified by the microstructures on the surface. However, this equation does not account for surfaces that are composed of two or more materials, and thus cannot be applied to chemically heterogeneous rough surfaces. Cassie and Baxter's [113] equation provides a reliable estimate for chemically heterogeneous surfaces composed of two materials:

$$\cos\ \theta' = f_1 \cos\ \theta_1^* + f_2 \cos\ \theta_2^* \tag{4.5}$$

in which θ_1^* is the contact angle of a fraction of surface area f_1, and θ_2^* is the contact

angle of the other fraction of surface area f_2, where $f_1 + f_2 = 1$. They applied this equation to the second behavior (*vide supra*) of liquids on rough surfaces (*i.e.*, air pockets arises from the microstructure on the surface) by assuming only a fraction (f) of the liquid drop is contacting the very top of the microstructures. This implies that the contact angle on such a surface is an average of the angles between the fraction of solid-liquid interface (f) and the vapor-liquid interface (1-f), which results in the modified equation:

$$\cos\ \theta' = f \cos\ \theta^*(1 - f) \tag{4.6}$$

Following the reasoning from this equation, the smaller the solid-liquid interface fraction f is, the higher the hydrophobicity of the rough surface. In other words, if the liquid drop was only contacting air, then the apparent contact angle θ' would be 180°. Subsequently, contact angle measurements not only provide a estimate of the surface energy/tension of the solid substrate, but can also provide a direct measure of aqueous wettability of the substrate.

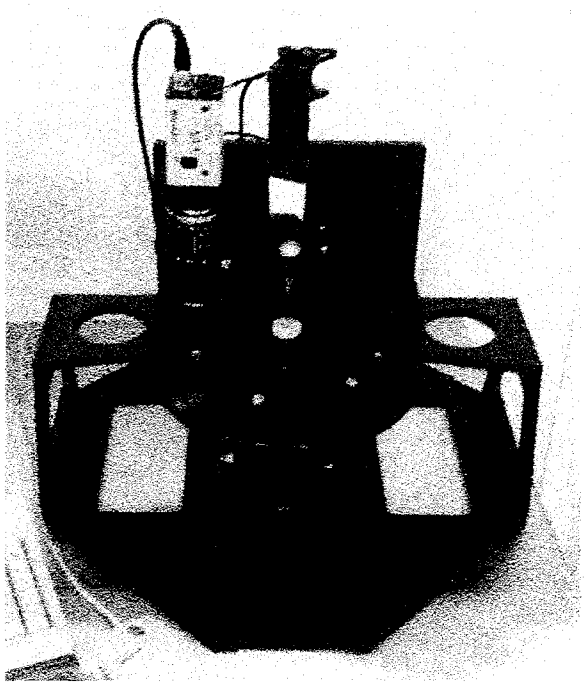

Figure 4.6: First Ten Angstroms FTA100 Series contact angle/surface energy analysis system.

On the basis of these principles, advancing aqueous contact angle measurements in the present study were performed using a First Ten Angstroms FTA100 Series contact angle/surface energy analysis system (Fig. 4.6) and the standard sessile drop method. As received, bare ITO exhibited an advancing aqueous contact angle (θ) of 85° using deionized water as the probing liquid (Fig. 4.7a). Upon treatment with oxygen RIE, θ = 0° consistent with a surface saturated with –OH. After treatment with a solution of alkyltrichlorosilane, the hydrophobicity of the flat ITO surface increased as evidenced by the advancing aqueous contact angle (*e.g.*, R = –CHCH2; θ = 111°), confirming derivatization of the ITO surface with covalently bonded organic moieties [61]. As-prepared GLAD films all show $\theta = 0°$. It is unclear if this surface property is the result of the GLAD porous structure, film surface chemistry or the most likely case, a combination of both. To ensure saturation of the surface with –OH moieties, GLAD films were treated with non-destructive oxygen plasma RIE before siloxane derivatization. Following assembly of organotrichlorosilane onto the GLAD films, all of the structural motifs were found to be extremely hydrophobic (helices: θ = 122°, slanted posts: θ = 124°, vertical posts: θ = 128°). A trend is observed from comparing the contact angles of the various structural motifs, *i.e.*, $\theta_{verticalposts} > \theta_{slantedposts} > \theta_{helices}$. However, the difference in these contact angles is within the measurement error of the CA system, and the effect of the structural motifs on the aqueous wettability of the films is not conclusive. A comparison of CAs for vinylsiloxane-functionalized flat ITO and GLAD films shows a significant increase in surface hydrophobicity with the introduction of a GLAD film (ITO vs. vertical pillar GLAD: 111° vs. 128°). Similar results were noted for substrates functionalized with

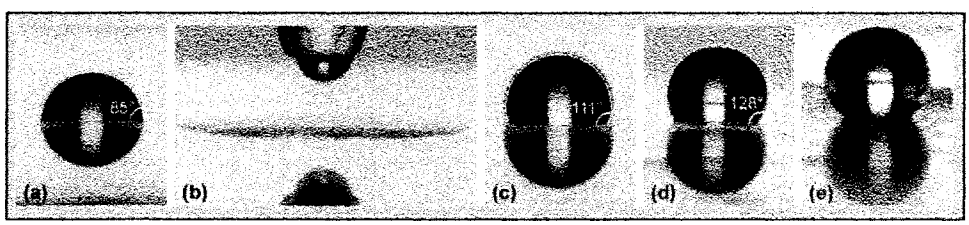

Figure 4.7: Advancing aqueous contact angle measurements of (a)bare ITO, (b) oxygen-RIE-treated ITO, (c)vinylsiloxane-derivatized ITO, (d) vinylsiloxane-derivatizedSiO_2 GLAD vertical posts on ITO, and (e)3,3,3-trifluoropropyl-trichlorosilane-derivatized SiO_2 GLAD vertical posts on Si100. This spectra is modified from [109].

octadecyltrichlorosilane (θ = 128°). Clearly, the differences seen in the hydrophobicity of flat ITO and GLAD substrates are a consequence of synergistic effects of high surface area columnar structures and the chemical properties of the siloxane bound alkyl surface moieties. To investigate the extent to which a surface could be rendered hydrophobic using this approach, 3,3,3-trifluoropropyl-trichlorosilane was self-assembled onto SiO_2 GlAD posts on Si{100} and bare Si{100} (using the general procedure noted in Chapter 3). Upon treatment with 3,3,3-trifluoropropyl-trichlorosilane, flat Si{100} surfaces were rendered hydrophobic (θ = 94°) while vertical pillar GLAD films (Figure 4.7e) were super-hydrophobic (θ >150°), once again confirming that the surface roughness introduced by GLAD pillars significantly increases the hydrophobicity of the substrate.

4.4 Cyclic Voltammetry

Cyclic voltammetry exploits electrochemistry to study the thermodynamics and kinetics of redox processes in organic and/or inorganic chemistry. This analysis technique is based on the operation of an voltammetric cell, which consists of three electrodes and an electrolyte. In cyclic voltammetry, one of the electrodes is called the working electrode, and in the present experiment, this electrode is the one that is under analysis. The second electrode is the reference electrode and a material that is usually inert to the electrochemical reaction is used for this electrode. As the name implies, all voltage and current measurements during the operation of the electrochemical cell are performed with respect to the reference electrode. However, a third electrode known as the counter electrode is required in cyclic voltammetry. This third electrode is largely used for large currents and/or low conductivity electrolyte solutions to avoid a potential drop at the working electrode caused by the internal resistance of the electrolyte. The standard three-electrode system (Fig. 4.8) along with the potentiostat/galvanostat is very important in cyclic voltammetry because it ensures that the potential applied is largely the same as the potential of the working electrode with respect to the reference electrode. This is done by using the galvanostat to adjust the currents passing through the counter and the working electrode until the potential at the working electrode corresponds to the potential applied. The potentiostat/galvanostat also records voltage and current simultaneously to produce the characteristic voltage-current

curve, referred to as the cyclic voltammogram.

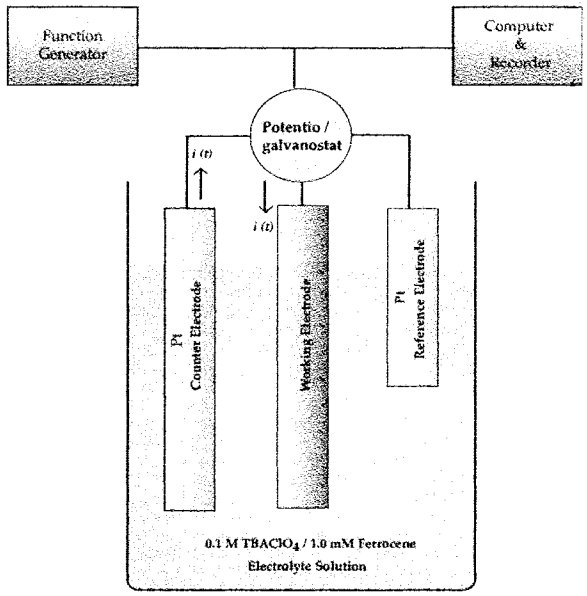

Figure 4.8: A representative schematic of a voltammetric cell.

In order for a voltammetric cell such as the one shown above (Fig. 4.8) to operate, the electroactive species in the cell must undergo a reduction-oxidation reaction (known as redox reaction). For any reduction (*i.e.*, gaining electrons) reaction to occur in the cell, there must also be an oxidation (*i.e.*, loss of electrons) reaction, and vice versa. Since an inert reference electrode is used in cyclic voltammetry, it is the electroactive species in the electrolyte that are reduced and oxidized throughout the operation of the cell. Typically, the electrolyte solution contains only a single electrochemical reactant that is either in its reduced or oxidized form. The reduction and oxidation of the this reactant during the operation of the voltammetric cell depends on the polarity and potential of the voltage applied. In both cases, the potential applied must be equal to the redox potential before reduction or oxidation will occur. The linear voltage sweep applied to the working electrode follows the waveform shown in Fig. 4.9. Note that the initial voltage potential (V_1) can be positive or negative. After the voltage reaches the switching potential, the polarity is reversed and the voltage returns linearly to its initial value [114, 115].

Generally, the current measured at the working electrode throughout the voltage sweep has two components: one is the heterogeneous charge transfer and the other is mass

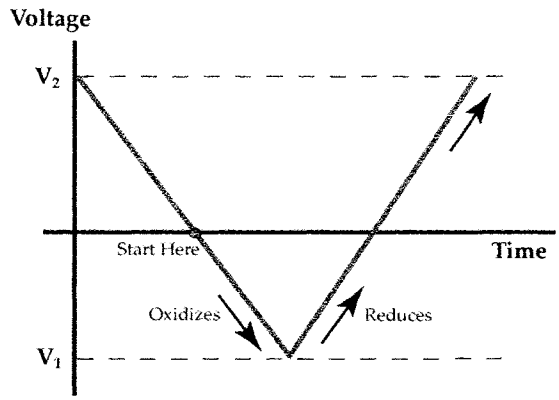

Figure 4.9: A representative waveform of a typical linear voltage sweep used in cyclic voltammetry to initiate redox reactions.

transport. Therefore, the characteristic shape of the voltammogram is a result of the voltage-dependent changes in the surface concentrations and the simultaneous diffusion processes of the ions in the electrolyte to the electrode surface. Following this reasoning, each redox system can then be identified by their characteristic shapes of voltammetric wave and unequivocal position on the potential scale.

In the case of a reversible cyclic voltammogram, the rate of charge transfer is much higher than the voltage sweep rate and a dynamic equilibrium of charges can be established at the electrode surface. Consequently, the current measured in this case is solely dependent on the diffusion of masses. For example, consider the electrochemical reactive species, ferrocene, in the electrolyte to be in its reduced form, Fe^{2+}. When the voltage is swept from zero potential (*i.e.*, the starting point denoted in Figure 4.9) to V_1, the equilibrium concentration of the reactant at the surface of the working electrode is shifted gradually from no conversion at the starting point to its oxidized form Fe^{3+} at V_1. This shift causes a concentration gradient at the surface of the electrode, resulting in the continuous diffusion of the reactant Fe^{2+} from the electrolyte to the surface of the working electrode. The working electrode then converts any reactant reaching its surface into its reduced form (Fe^{2+}) and a flow of net anodic current from the working electrode to the electrolyte results. This anodic current increases exponentially with potential, converting more and more reactant to its oxidized form. The current peak arises when most of the reactant has been converted to its oxidized form (*i.e.*, the concentration of the reduced form of the

reactant, Fe^{2+}, at the surface of the electrode becomes negligibly small). At this point, the diffusion layer at the surface of the working electrode has grown sufficiently large such that most of the reactant flux cannot reach the electrode surface. Hence, current curve decays virtually independent of the potential as the concentration gradient decreases and little of the reactant is converted. At the switching potential V_1, the voltage sweeps in the opposite direction (*i.e.*, from V_1 to V_2), and analogous phenomena occurs. In this reverse direction, the electrolysis product or oxidized form of the reactant Fe^{3+} is converted to back to the original form Fe^{2+}. The current now flows from the electrolyte to the working electrode and the peak occurs when most of the electrolysis product is oxidized and a negligible concentration of the product is present in the electrolyte. This cathodic current then decays as the diffusion layer continues to expand while concentration gradient decreases. Hence, the full voltammogram for a reversible process consists of two important current peaks: a positive current peak for the reduction process and the negative peak for the oxidation process of the electrolyte. Since all mass transport of the reducible or oxidizable electroactive species occurs through diffusion, a 0.1 M solution of a ground or supporting electrolyte must be added to the electroreactive electrolyte solution to ensure solution conductivity and eliminate migration currents. The recorded current values for all applied voltages (*i.e.*, the y position of the voltammogram) may be shifted by changing the voltage scan rate. A slow voltage scan rate will increase the time the potentiostat/galvanostat takes to record the voltammogram. The increase in time allows the diffusion layer to expand further away from the electrode compared to a faster voltage scan rate. Consequently, the accessible electrode surface to the reactant flux is considerably smaller at a slow rate than at a higher rate, and the recorded current values increase with scan rate (*i.e.*, the voltammogram shifts up as scan rate is increased). Yet, the x position or the potential at which the current peaks occur should not change with scan rate if the redox reaction is reversible. Also, for the redox process to be reversible, the potential separation between the two current peaks is constant [114].

In contrast, if charge transfer occurs at an extremely slow rate relative to voltage scan rate, no concentration gradient is produced at the electrode surface and the kinetics are too slow to establish an equilibrium. In this case, the current is primarily controlled by

the charge-transfer reaction instead of mass diffusion, and the process becomes quasi-irreversible or irreversible. For irreversible processes, usually only one of the reduction or oxidation reactions can be measured and the voltammogram will only have one of the current peaks. In the quasi-irreversible case, the current is determined by both charge transfer and mass transport processes, but it is the voltage scan rate that determines which of these two processes become the dominant effect at the electrode. In both cases, the voltage position at which the peaks occur will alter with voltage scan rate and the separation between the current peaks are no longer constant.

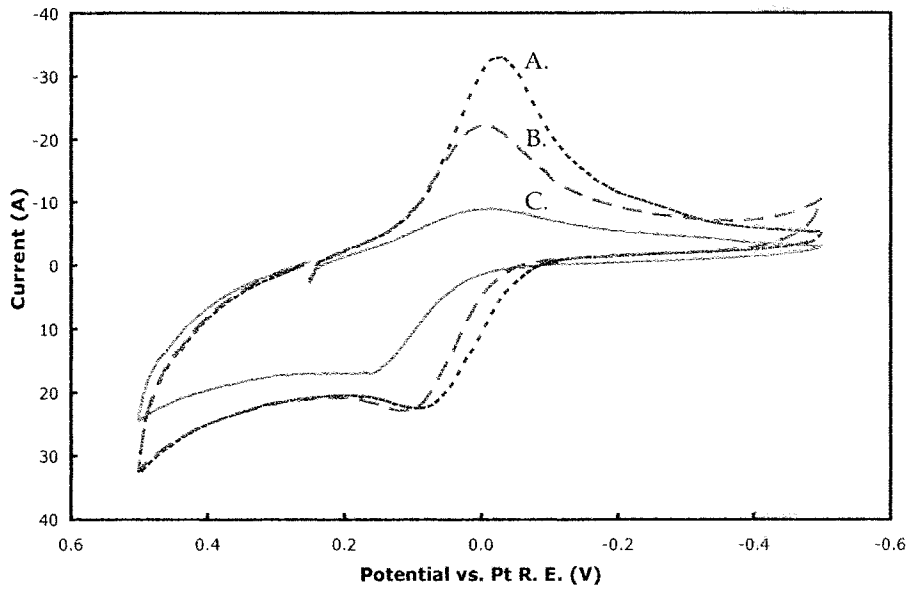

Figure 4.10: Cylic voltammograms of 1.0 mM ferrocene solution in 0.1 M $TBAClO_4$ supporting electrolyte using (A) bare ITO-coated glass substrate, (B) helical SiO_2 pillars on ITO, and (C) vinylsiloxane-dervatized helical SiO_2 pillars on ITO as working electrodes.

It is of interest and importance to the project that trichlorosilane reagents penetrated into the columnar GLAD structures and reacted with the underlying support substrate. To investigate this possibility, GLAD films on ITO (as-deposited and functionalised) were used as working electrodes in a standard three-electrode electrochemical cell. A 1.0 mM ferrocene solution is used as the electrochemical probe here and it has previously been used as an electrochemical probe to investigate the surface functionalization of flat ITO surfaces [61]. Cyclic voltammetry (CV) was performed with an EG&G Model 263A

Instruments Potentiostat/Galvanostat. A 0.1 M $TBAClO_4$/acetonitrile was used as the supporting electrolyte, and Pt wires were used as the pseudo-reference electrode and counter electrode. All voltammograms were obtained using a voltage scan rate of 100 mV/s. Cyclic voltammetry experiments using unfunctionalized ITO and GLAD films as the working electrode show reversible Fe^{2+}/Fe^{3+} oxidation/reduction characteristic of the ferrocene probe (Fig. 4.10A and B). Upon functionalization with vinylsiloxane, the reversible ferrocene/ferrocenium redox process was suppressed and replaced by an irreversible oxidation process identical to that is seen for analogous flat ITO electrodes functionalized with a vinyl siloxane molecular layer [57, 61]. From this observation we can conclude that vinyltrichlorosilane penetrates into the GLAD structure to chemically modify the underlying substrate. As an extension of this observation, it is presumable that the interior pillar surfaces are also derivatized.

4.5 Chapter Summary

The surface chemistry of SiO_2 GLAD films have been effectively tailored using a well-established siloxane-based chemical approach. Advancing aqueous contact angle measurements indicate that the high surface area of GLAD films, combined with controlled surface chemistry, provides a straightforward, effective method for preparing substrates whose hydrophobicity exceeds that of their flat counterparts. The electrochemical studies also suggest that the siloxane reagents penetrate into the GLAD film to form a three-dimensional matrix with controlled surface chemistry. Clearly, the chemical structure of the surface modifier has a great influence on the hydrophobicity of the functionalised GLAD films. This dependency is illustrated by the contact angles of SiO_2 pillars bearing R=–OH, $-CH_2{=}CH_2$, $-CH_2(CH_2)_{16}CH_3$, and $-CH_2CH_2CF_3$ for which θ lies in the range of 0 to >150°. As demonstrated, hydroxyl moieties render the surface hydrophilic, simple hydrocarbon chains render surface hydrophobic, and fluorinated surface modifiers results in superhydrophobicity. This nanoscale control of SiO_2 GLAD film surface properties have facilitated interfacing these films with hydrophobic, functional organic materials and device applications such as chemical sensors and optical filters.

5

The Utility of Solution and Vapour-phase Chemical Functionalisation Methods on GLAD

This chapter compares the effectiveness of solution and vapour phase functionalisation methodologies. The sensitivity of GLAD films to trace of water impurities in the solvent used in the solution functionalisation method is discussed. To minimise problems arising from the use of solvents, the simpler and more straightforward method of vapour-phase functionalisation

was investigated as an alternative to solution-based surface functionalisation of GLAD films. Here, 3,3,3-trifluoropropyl-trichlorosilane ($CF_3CH_2CH_2SiCl_3$) and 7-octen-1-yl-trimethoxysilane ($H_2C{=}CH(CH_2)_6Si(OCH_3)_3$) reagents were used to tailor the surface chemistry of 2.0 μm helical metal oxide (TiO_2, SiO_2, and Al_2O_3) GLAD films via solution and vapour-phase functionalisation methods. The effectiveness of the two methods was compared using various characterisation techniques including SEM, XPS, and advancing aqueous contact angle measurements.

5.1 Effects of Solution Functionalisation Methodology

SEM images of the previously described solution-base functionalised GLAD films show that the columnar nanostructures stay intact throughout the functionalization process. However, throughout the course of studies on various solution functionalisation processes, it was discovered that GLAD films are highly sensitive to traces of impurities in the solvent. In the presence of trace water impurities, which arise when freshly distilled solvents are not used in the functionalisation procedure, the GLAD pillars tend to agglomerate into a "haystack" structure (Figure 5.1b). Following this observation, other extremely polar compounds (*e.g.*, water, methanol) with high surface tension were used to wet the GLAD films and the same agglomeration effect was noticed. This observation was similar to, but less pronounce than the "nanocarpet" effect reported by Fan *et al.* [37]. They believe that the strong capillary force produced by the highly polar liquid wetting into the voids of the high aspect ratio (~50:1) pillars leads to the deformation of the pillars. Another possible explanation may be that the evaporation of water (a liquid with high surface tension) from the film during the annealing process strains the pillar structures, resulting in agglomeration of the pillars into the haystack structure. The formation of these haystacks and the loss of regular film structure could hinder many device applications based on this property of the GLAD films. However, the cause for the agglomeration of the GLAD pillars have not been studied in detail and further examination is required for conclusive explanations to be drawn.

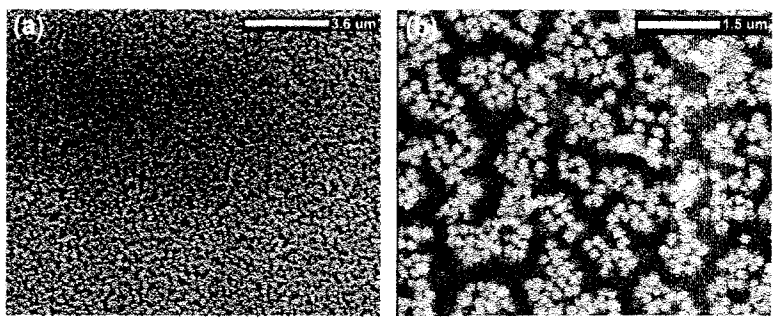

Figure 5.1: Representative top view SEM images of (a) non-treated, and (b) solution-base vinyl-trichlorosilane-derivatized SiO_2 film with traces of water impurities in the solvent.

To minimise pillar agglomeration, solvent waste, and demonstrate flexibility in the

present approach for tailoring GLAD film surface properties, the current studies were extended to vapour-phase functionalisation of silica, titania, and alumina GLAD films. SiO_2, TiO_2, and Al_2O_3 helical GLAD films on Si{100} and glass substrates were placed in a vacuum desiccator with an open vial containing 1.0 mL of the desired, volatile organotrichlorosilane reagent. The desiccator was evacuated and filled with the reagent vapour of choice and the substrates were allowed to react for 48 hours.

5.2 Scanning Electron Microscopy Analysis

Side view SEM micrographs of solution and vapor-phase treated SiO_2, TiO_2, and Al_2O_3 helical GLAD film (Figure 5.2) were used to inspect any morphology changes in the film arising from the functionalisation procedure. As expected, the SEM images of solution and vapour-phase surface functionalised SiO_2 and TiO_2 GLAD films on show unchanged film microstructure no agglomeration of the pillars resulting from the functionalization procedure (Figure 5.2b, c). Similar results were noted for solution-base derivatization of Al_2O_3 film (Figure 5.2d). In stark contrast, SEM images of vapor-phase treated helical Al_2O_3 film indicated the voids of the GLAD film were almost completely filled (Figure5.2e, f), though some evidence of the underlying film nanostructure can still be seen. Clearly this is a significant change from the solution functionalized or non-treated film. This observation is consistent with well-established reactivities of SiO_2, TiO_2, and Al_2O_3 with the byproduct of the organotrichlorosilane reaction, HCl. In particular, SiO_2 and TiO_2 are known to be resistant to HCl whereas Al_2O_3 reacts with HCl to neutralise it. This alone makes the alumina nanostructures more susceptible to degradation in this procedure. It is conceivable that that the aluminium oxide GLAD film reacts with HCl to form a complex aluminium chloride compound. As this new compound was exposed to ambient conditions, the hydroxyl groups in air binds to the aluminium chloride complex to yield hydrated alumina [116]. This reaction causes the pillars to swell and expand until the film voids are completely filled. It is unfortunate that this side reaction leads to the destruction of the alumina films and the simple desiccator used in the present functionalisation process cannot actively exhaust gaseous byproducts since it only has one inlet. However, this reaction does support the electrochemical observations earlier that the siloxane-based chemistry proceeds

to functionalise the interior pillar surface as well as the underlying substrate surface as illustrated by the uniform broadening of the alumina pillars in Fig.5.2f. Similar pillar broadening effect was not observed for the solution functionalised alumina film because the reactivity of HCl in reduced in organic media.

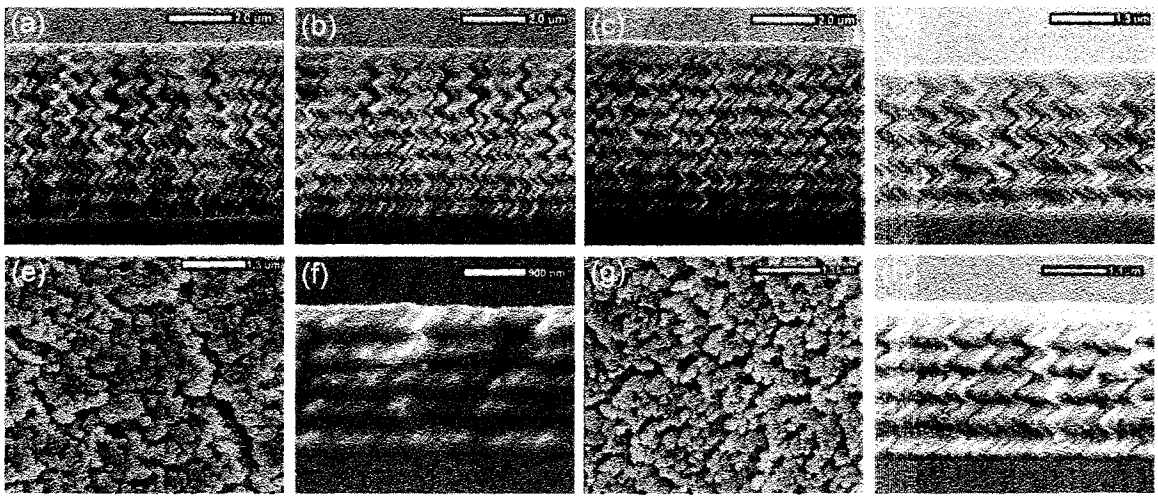

Figure 5.2: Representative SEM images of (a) untreated metal oxide film, (b)solution, and (c)vapour-phase 3,3,3-trifluoropropyl-trichlorosilane-derivatized SiO_2 and TiO_2 helical GLAD film; (d) solution, and (f) vapour-phase 3,3,3-trifluoropropyl-trichlorosilane-derivatized Al_2O_3 film, and (e) is the corresponding top view to (f). (g) and (h) are top and side view SEM images of the mark observed on the film after the evaporation of the water drop from contact angle measurements, respectively.

When contact angle measurements were performed on the vapour-phase treated alumina film via dispensing a drop of distilled water on to the surface, the water drop was observed to gradually spread on the surface. The film surface was then blown dry using a stream of nitrogen and a water mark corresponding to the location of the drop was observed to remain on the surface. A SEM micrograph of the water-marked alumina film (Figure 5.2g, h) clearly showed the voids of the film being much less filled than prior to its contact with water (Figure 5.2f). This observation suggests that the product of the reaction between HCl and alumina is water soluble, which is consistent with the hypothesis that the alumina film is converted into hydrated alumina, and hence parts of the film can be washed away by water.

5.3 X-ray Photoelectron Spectroscopy Characterisation

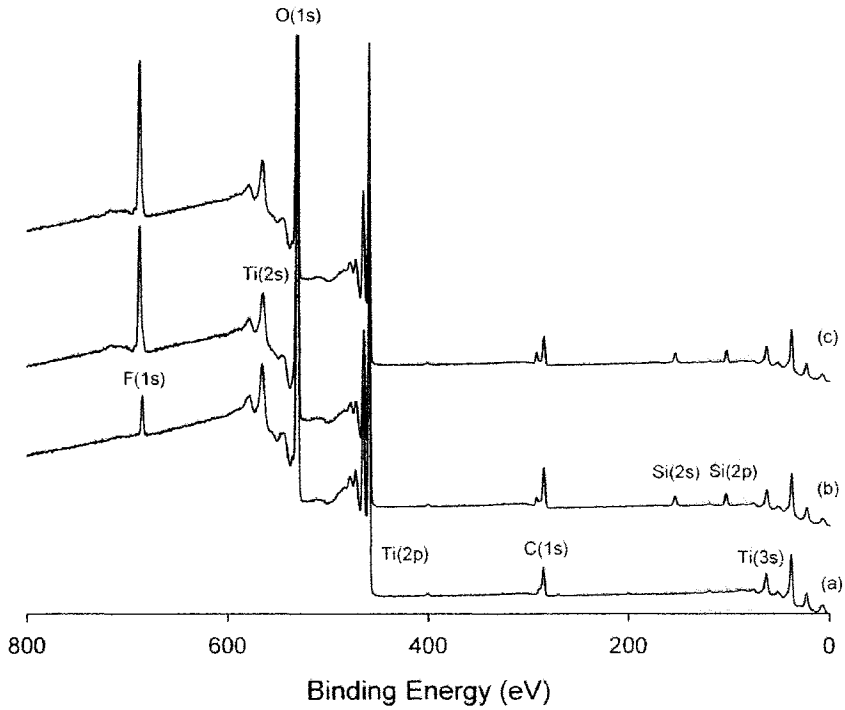

Figure 5.3: X-ray photoelectron spectroscopy of (a) untreated, (b) solution, and (c) vapour-phase 3,3,3-trifluoropropyl-trichlorosilane-derivatized helical TiO_2 film prepared on Si100 substrates.

XPS analysis of vapour functionalised TiO_2 and SiO_2 GLAD films show emissions arising from the surface modification that are more intense than the same signals noted for analogous solution derivatized samples. XPS of unmodified TiO_2 films (Figure 5.3a) prepared on Si{100} substrates show characteristic Ti(2s), Ti(2p), Ti(3s) and O(1s) signals. The small C(1s) emission observed in this spectrum can be attributed to adventitious carbon arising from the melting of the carbon crucible holding the source material during deposition. Upon functionalization with 3,3,3-trifluoropropyl-trichloroislane, a slight decrease in the emission intensity arising from the GLAD pillars and a concomitant increase in C(1s), appearance of Si(2s), Si(2p) and F(1s) emissions were noted in the XPS spectra of vapor-phase (Figure 5.3c) surface treated titania film. This is consistent with the attachment of organic moieties onto the surface of the film. Similar results were noted for SiO_2 films prepared on Si{100} substrates. Emissions from the solution

treated Al_2O_3 (Figure 5.4 b) films were similar to the solution spectra observed for the other two metal oxides, and the appearance of F(1s), Si(2s), Si(2p) and the simultaneous increase in C(1s) signal supports a change in the surface chemistry of the GLAD film as stated before. However, a significant decrease in all characteristic alumina emissions, with respect to the untreated or solution functionalized alumina, is observed from the vapor-phase functionalized Al_2O_3 spectra (Figure 5.4c). Yet, the F(1s) and C(1s) emissions of the vapor-phase treated Al_2O_3 film were substantially higher than the untreated or solution treated alumina film. This is consistent with the earlier presumption that Al_2O_3 has reacted with HCl, and hence the strong characteristic signals from Al_2O_3 film were not observed as expected. Furthermore, this noticeable decrease of Al(2s), Al(2p) and O(1s) emissions implies a decrease in the mass concentration of aluminium and oxygen in the alumina film, which in turn means an increase in the mass concentration of F and C in the aluminum oxide film.

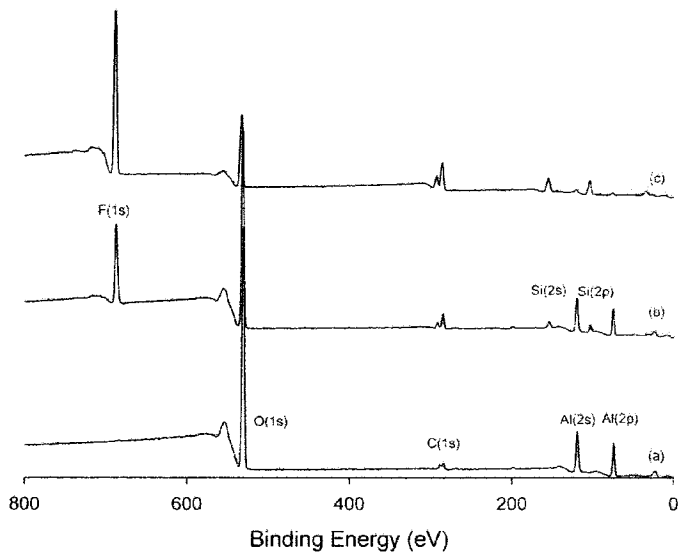

Figure 5.4: X-ray photoelectron spectroscopy of (a) untreated, (b) solution, and (c) vapour-phase 3,3,3-trifluoropropyl-trichlorosilane-derivatized helical Al_2O_3 film prepared on Si{100} substrates.

5.4 Organotrimethoxysilane Surface Functionalisation

To eliminate the detrimental side reaction of HCl with Al_2O_3 GLAD films, surface functionalisation of GLAD films with organotrimethoxysilane reagents were investigated. These reagents were previously used to functionalise flat Al_2O_3 substrates [117] and beads [118] via solution-based methods. Organotrimethoxysilane reagents are particularly promising for alumina GLAD film surface modification because methanol is the only byproduct of the reaction and will not react with the alumina film. Using the same solution and vapour phase procedures described for alkyltrichlorosialnes, alumina films were surface functionalised with 7-octen-1-yl-trimethoxysilane. The SEM micrograph in Fig.5.5a is a SEM representative image of pre- and post- solution and vapour-phase trimethoxysiloxane-derivatized Al_2O_3 film. Clearly, no structural variations or filling of the voids is seen. This is supports with the previous assumption that the filling of the film's void volume is caused by the reaction between HCl and Al_2O_3. Hence, when the film material is inert to the byproduct, the nanostructures of the film will remain intact throughout the functionalisation procedure.

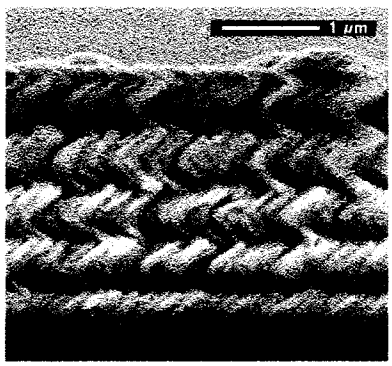

Figure 5.5: A representative SEM image of pre- and post- solution and vapour-phase 7-octen-1-yl-trimethoxysilane functionalised Al_2O_3 film.

The solution and vapour trimethoxysiloxane-derivatized alumina film XPS sptectra show characteristic alumina signals, confirming that the alumina surface is not susceptible to reaction with the methanol byproduct. In addition, a significant increase in C(1s), and the appearance of Si(2s) and Si(2p) emissions were noted in both of the XPS spectra presented in Fig. 5.6. Therefore, the vapour-phase chemical functionalisation method

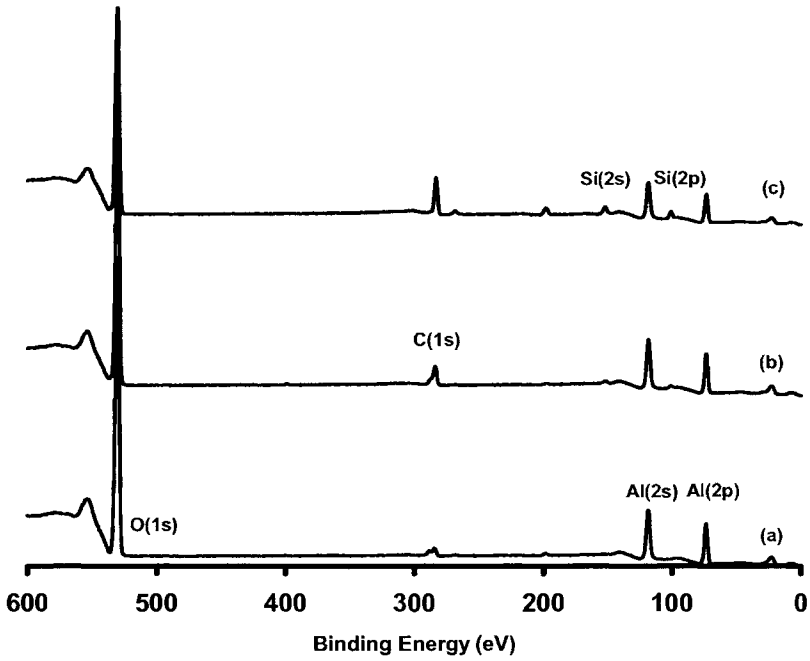

Figure 5.6: X-ray photoelectron spectroscopy of (a) untreated, (b) solution, and (c) vapour-phase 7-octen-1-yl-trimethoxysilane-derivatized helical TiO_2 film prepared on Si100 substrates.

is still an effective method for tailoring the surface properties of GLAD films as long as the film material is not susceptible to reacting with the byproduct of the functionalisation reaction. A comparison of the two methoxysiloxane-derivatized alumina spectra in Fig. 5.6 suggests that vapour-phase treatment methods is more effective than the solution method since the C(1s), Si(2s), and Si(2p) peaks have noticeably higher intensity in the vapour-treated alumina spectra than its solution counterpart. In addition, XPS analysis of all films derivatized with solution and vapour phase protocols with organotrichlorosilanes and organotrimethoxysilanes show an expected appearance of Si(2s) and Si(2p) peaks, supporting a surface siloxane linkage.

5.5 Advancing Aqueous Contact Angle Measurements

The following table summarises the contact angle measurements for untreated, solution and vapour phase chemically modified metal oxide GLAD films. The chemical structure of the two reagents used to tailor the surface chemistry of the GLAD films in the present study is given in Figure 5.7.

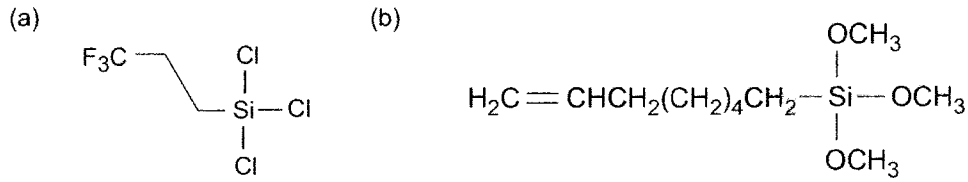

Figure 5.7: The chemical structure of (a)3,3,3-trifluoropropyl-trichlorosilane, and (b)7-octen-1-yl-trimethoxysilane. The latter reagent is referred to as $C_{11}H_{24}O_3Si$.

Table 5.1: Advancing aqueous contact angle (CA) comparison of untreated, solution and vapour phase modified SiO_2, TiO_2, and Al_2O_3 helical GLAD films.

Materials	CA of Untreated & RIE-treated	CA of $CF_3CH_2CH_2SiCl_3$ Treated		CA of $C_{11}H_{24}O_3Si$ Treated	
		Solution	Vapour	Solution	Vapour
SiO_2	0°	120°	121°	–	–
TiO_2	0°	67°	118°	–	–
Al_2O_3	0°	81°	94°	33°	52°

As-deposited and oxygen plasma RIE treated metal oxide GLAD films exhibit an advancing aqueous contact angle of $\theta = 0°$ (Fig.5.8a) as previously depicted in Chapter 4. Following the assembly of 3,3,3-trifluoropropyl-trichlorosilane, the metal oxide surfaces of present structures exhibit differing degrees of hydrophobicity. Solution and vapor-phase functionalised helical SiO_2 film were observed to be very similar (120° vs 121° in Table5.1). However, comparing the contact angle of these solution modified helical silica films (Figure 5.8b) to the vertical post silica films modified with the same fluorinated-trichlorosilane reagent in the previous chapter (Figure 5.8e), it is clear that the vertical pillars exhibit significantly greater hydrophobicity than helices (*i.e.*, $\theta_{pillars} > 150°$, $\theta_{helices}$

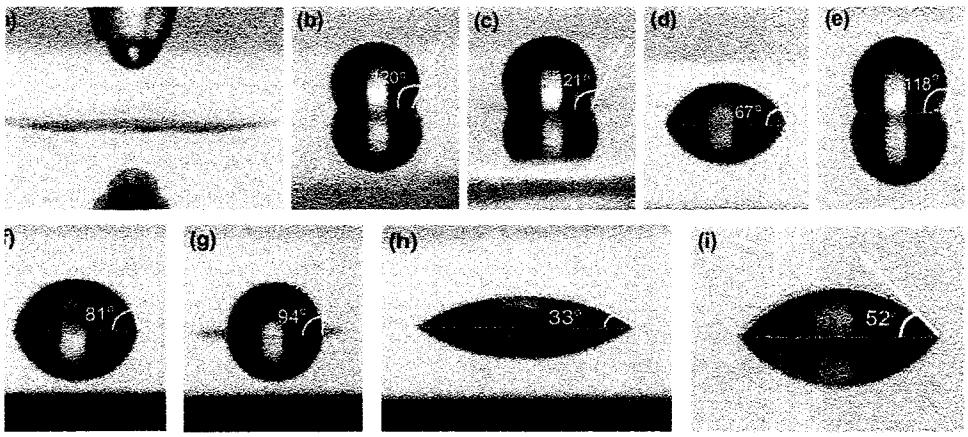

Figure 5.8: Representative aqueous advancing contact angle measurements of (a) untreated, (b) solution, and (c) vapour-phase 3,3,3-trifluoropropyl-trichlorosilane-derivatized SiO_2; (d) solution, and (e) vapour-phase 3,3,3-trifluoropropyl-trichlorosilane-derivatized TiO_2; (f) solution, and (g) vapour-phase 3,3,3-trifluoropropyl-trichlorosilane-derivatized Al_2O_3; (h) solution, and (i) vapour-phase 7-octen-1-yl-trimethoxysilane-derivatized Al_2O_3. All of the films were of helical structures prepared on Si100 substrates.

= 120°). From straightforward geometrical considerations, it can be seen that helices have greater contact area with the water droplet than the vertical pillars. According to the Cassie and Baxter's modified equation (Equation 4.6), the greater the liquid-solid contact surface is, the lower the hydrophobicity would be for a rough surface. Hence, it is reasonable that the modified vertical pillars exhibit greater hydrophobicity than similarly modified helices. Furthermore, considering the structural motif of the two films, vertical post nanostructures have easily accessible surface area for the oxygen ions in RIE treatment, whereas the helical structure may have hidden areas where the oxygen ions cannot reach. This suggests the density of the hydroxyl groups on the surface of the helical structures may be less than the vertical post structures. Since the maximum reactivity between the film surface and the organosilane reagents depends on the density of hydroxyl groups on the that surface, a higher density of –OH implies that the surface can be more effectively functionalised. Again, this supports the greater hydrophobicity observed from the surface modified vertical posts than the similarly treated helical film.

Though the vapour and solution phase functionalisation of SiO_2 films produce nearly identical advancing aqueous contact angles, this is not the case for the analogous treated TiO_2 and Al_2O_3 films. The solution 3,3,3-trifluoropropyl-trichlorosilane treated alumina

structure exhibit advancing aqueous contact angle of 76° while vapour functionalisation resulted in destruction of the film. A significant difference between solution and vapor phase 3,3,3-trifluoropropyl-trichlorosilane derivatized TiO_2 contact angles, $\theta_{solution}$ = 76° and θ_{vapour} = 118°, respectively was noted. θ = 76° for solution treated TiO_2 is consistent with the results observed by Advincula *et al.* for solution-based functionalisation of high surface area sol-gel derived TiO_2 [119]. It is unclear why the solution functionalised films are less hydrophobic than their vapour phase derivatised counterparts. However, a qualitative comparison of the relative intensities of Si(2s) and Si(2p) XPS emissions of the solution and vapour phase derivatised titania film suggest that there is a greater Si concentration at the surface of the vapour modified film. Another plausible explanation may be the greater accessibility of the GLAD film internal structure afforded to the vapour phase orgranic moieties. Also, the reactant solution used in vapour-phase functionalisation was used as-received whereas the reactant solution was diluted using dry toluene to a concentration of 20 mM in solution functionalisation. The higher reagent concentration in vapour-phase functionalisation may lead to the chemisorption of significantly more reactant to the film surface when compare to solution functionalisation. The precise reason for the difference between the contact angles measured on vapor-phase and solution treated TiO_2 and Al_2O_3 film is unknown and a detailed investigation would be needed to explain this phenomenon. Contact angle measurements of trimethoxysiloxane-derivatized Al_2O_3 film (Figure 5.8h and i) demonstrate that a more hydrophobic surface, compared to the non-treated film ($\theta = 0°$), is achieved. However, the greater hydrophobicity of the vapour-phase functionalised film relative to its solution counterpart (*i.e.*, θ_{vapour} = 52° vs $\theta_{solution}$ = 33°) is once again observed in the trimethoxysilane functionalised film.

5.6 Chapter Summary

To summarise, agglomeration of GLAD pillars arising from traces of water impurities in solvents used in solution surface functionalization have been effectively prevented by extending the present approach to the vapour-phase functionalisation method. SEM micrographs of pre- and post-functionalised metal oxide films indicate the GLAD structures remain unchanged throughout the two functionalization processes, with the

exception of alumina. Though the byproducts from the vapour functionalisation process reacted with alumina to completely fill the voids of the film, it was demonstrated that alumina films can still be effectively tailored with no structure deterioration by vapour-phase functionalizing with organotrimethoxysilane. XPS results further confirmed the hypothesis that the film structure will not deteriorate as long as the film material is not susceptible to react with the byproducts of the functionalisation processes. Advancing aqueous contact angle measurements and XPS results suggest that vapour-phase functionalisation may be a superior method for tuning the surface energies of GLAD films since surfaces with greater content of the organic moieties and greater hydrophobicity than its solution counterpart can be achieved with this method. In addition, vapour-phase functionalisation is a more straightforward, inexpensive, and versatile method that eliminates the use of solvents,making it the ideal method for tuning the surface properties of GLAD films and other substrates.

6

Applications and Future Directions

Up until now, this thesis had focused on the chemical tunability of various GLAD films through surface functionalisation methods. In the next few sections, the first application of surface functionalisation to GLAD-produced humidity sensors and optical band-bass filters is described in detail. The effects of surface functionalisation on the devices' sensitivity to relative humidity are reported, along with other potential applications of surfaced treated GLAD films. The latter part of this chapter discusses recommendations the author has for future experiments arising from this project. Finally, a summary of all the work and results presented in this thesis is given.

6.1 Application of Surface Treated GLAD Films

Some of the most important properties of a humidity sensor include high sensitivity, broad range of operation for both humidity and temperature, small hysteresis, low cost, and fast response time among others. The response time of a sensor refers to the time it takes the sensor to respond to a step change in the humidity. Thus, the rate at which successive measurements can be made by a humidity sensor is limited by the response time of the sensor. It has been recently demonstrated that GLAD-based capacitive humidity sensors

have nominal response times of 40-100 ms [44, 120]. This is a significant decrease from the 3 s response time of typical commercial humidity sensors, and it is doubtless the result of the high porosity and high surface area created by the GLAD nanostructures. However, the large pores in the GLAD film also makes the GLAD-based sensors less sensitive to changes in relative humidity, especially in the lower humidity regions. Since surface functionalisation methodologies can vary the degree of surface hydrophobicity or hydrophilicity by tailoring the surface chemistry of GLAD nanostructures, it may be an ideal method for controlling the sensitivity of GLAD-based humidity sensors.

In an attempt to improve the sensitivity of the GLAD-based sensor in the lower regions of humidity, a titania GLAD sensor was treated with O_2 plasma RIE to increase the hydrophilicity of the film. In theory, increasing the hydrophilicity of the GLAD film will increase the film's affinity for water, and may enhance water adsorption even at low humidity levels. As described before, the RIE process is known to saturate the surface of substrates with hydroxyl (-OH) moieties, which has the strongest affinity for water. Hence, RIE appears to be the best method for rendering surfaces extremely hydrophilic. Following 90 s of RIE treatment, the titania GLAD sensors were tested in a simple humidity chamber [121] and the capacitive responses were compared to the ones obtained pre-treatment. Advancing aqueous contact angle measurements showed contact angles (θ) of 0° for untreated and RIE-treated alumina sensor (Fig. 6.1). No noticeable differences were observed in the comparison of the pre- and post-RIE treated sensor's capacitive responses. This can be attributed to the fact that the alumina film was relatively hydrophilic prior to RIE treatment, and the hydrophilicity of the film simply cannot be increased sufficiently by RIE treatment to change the capacitive sensor response. In addition, the large pore size of GLAD films requires a corresponding high value in water vapour pressure before capillary condensation occurs. Hence, it is not too surprising that the RIE treatment did not have significant influences on the sensor response.

Subsequently, the titania GLAD sensor was rendered hydrophobic ($\theta = 98°$) via vapour-phase surface functionalisation using 3,3,3-trifluoropropyl-trichlorosilane as the chemical reagent. This functionalised sensor was tested in the same humidity chamber as before and its capacitance response, measured over a broad range of humidity levels, was compared

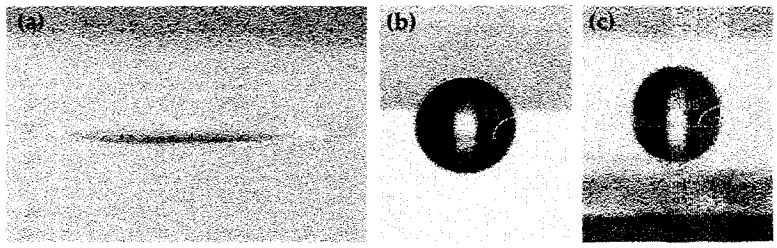

Figure 6.1: Representative aqueous advancing contact angle measurements of (a) untreated titania humidity sensor and optical rugate filter, and vapour-phase 3,3,3-trifluoropropyl-trichlorosilane-derivatised TiO_2 (b) humidity sensor and (c) band-pass rugate filter.

with the response curve of the unfunctionalised sensor. It was observed that the response of the functionalised sensor was completely insensitive to changes in humidity indicating the lack of water adsorption at the surface of the sensor. This implies that the degree of hydrophobicity of the chemical treated sensor is sufficient for inhibiting water vapour adsorption at all levels of humidity. Since capacitive sensors operate by having humidity dependent capacitance (*i.e.*, greater the amount of adsorbed water vapour, higher the capacitance measured), a lack of water vapour adsorption results in no significant change in capacitance [122]. Similar results were obtained for alumina GLAD sensors functionalised by solution-phase vinyl-trichlorosilane. The effectiveness of the surface functionalisation method for tailoring the surface chemistry of GLAD films is once again demonstrated by turning off the capacitive response of GLAD-fabricated humidity sensors. Furthermore, this surface functionalisation method opens many doors to future studies on various gas and chemical sensors. For example, it can be used in the fabrication of GLAD-based gas sensors by attaching a chemical reagent to the surface of the GLAD nanostructures that would selectively sense the desired substance through preferential adsorption.

Though the ability to inhibit the sensors' sensitivity to water by rendering the film surface hydrophobic is not useful in improving the performance of a humidity sensor, but it is interesting in consideration of humidity sensitive optical devices. Hence, the dependence of a GLAD-fabricated titania optical band-pass rugate filter's [42] optical response on changes in relative humidity was examined in the same humidity chamber as described before. It was noted that the position of optical bass band shifted significantly in wavelength as the humidity levels increased in the chamber. To prevent the response of the GLAD filter

to shift with humidity, vapour-phase surface functionalisation method was applied to the filter, and the surface of the GLAD filter was rendered extremely hydrophobic (θ = 109°) using 3,3,3-trifluoropropyl-trichlorosilane. The optical responses of post-functionalised titania optical filter yield a desensitized filter with no major shifts in the pass band at all humidity levels. Hence, the optical filter's sensitivity to humidity was successfully inhibited by tailoring the surface chemistry of the GLAD film.

6.2 Future Experiments

Aside from the applications described above, there are countless additional avenues of exploration as well as potential applications for tailoring the surface properties of GLAD films. For example, it has been demonstrated that helical structured GLAD films are chiral and its optical activity can be enhanced by impregnating the voids of TiO_2 GLAD films with organic liquid crystalline materials [123]. Because the liquid crystals (LC) are hydrophobic and the titania films are relatively hydrophilic, there is a surface energy mismatch at interface of the two materials, and thus, it is very difficult to embed the LCs into the film. A potential experiment can be to tailor the surface energy of the GLAD films such that it would match well with the LCs (*i.e.*, rendering the film surface hydrophobic), and thus allowing the LCs to flow more readily into the voids of the film. This will require testing with several organic functional materials with varying chain lengths and hydrophobicity in order to obtain the best matched surface energy possible. The hydrophobicity of the functionalised GLAD film and the attachment of the organic moieties can be determined by contact angle measurements and XPS analysis, respectively.

The large accessible surface area, high porosity, and the ability to control that porosity, make GLAD films ideal for sensing applications. Thus, the field of GLAD-fabricated sensors is filled with opportunities and it has the best potential for commercialisation. In the future, the application of surface functionalisation can be extended to various chemical gas sensors including carbon monoxide and volatile organic compounds (VOC). Because surface functionalisation is extremely versatile, a wide range of chemical reagents can be used to tailor the surface chemistry of GLAD films until the appropriate chemical is discovered for selective sensing of a certain compound. For example, in order to create a

carbon monoxide sensor, the surface chemistry of the GLAD film might be first tailored with 2-cyanoethyl-trichlorosilane, and subsequently attaching an iron porphyrin molecule to the tail group (CN) of the first chemical reagent. CO is known to attach to the iron, and once it attaches to the iron, the colour of the functionalised film may change (*i.e.*, the adsorption band of the iron porphyrin derivatised GLAD shifts with the attachment of CO molecules), indicating the presence of carbon monoxide. In the case of VOCs, TiO_2 GLAD films can be functionalised to varying degrees of hydrophobicity in order to sense a certain group of VOCs. For instance, the films can be made slightly hydrophobic for VOCs such as methanol and isopropanol. On the other hand, they can be tailored to be extremely hydrophobic for compounds such as toluene and hexane.

There are many other potential research ideas that can be explored with surface functionalisation in GLAD including improving the wetting of GLAD-fabricated organic thin films on silicon wafers, glass and ITO coated glass substrates by better matching the surface energies of the organic evaporant material and the substrate. Once again, a broad range of organic chemicals will need to be tested in this experiment. The goal in this experiment would be to obtain a graph of the wettability of organic materials deposited using GLAD with respect to hydrophobicity of the substrates. These functionalised film are also well suited for catalytic and biosensor applications. Very little amount of work has been placed into the investigation of the possibility of utilizing these GLAD films as cataylsis or biologic devices; consequently, there is much room for exploration in the these two fields.

6.2.1 Summary

In this thesis, the chemical tunability of various metal oxide GLAD films was explored using solution and vapour-phase surface functionalisation methodologies. First, SiO_2 films of vertical, slanted and helical structures were functionalised using solution siloxane-based surface chemistry. SEM images of pre- and post-solution-functionalised GLAD films showed no structural changes throughout the derivatization processes as long as there was no water impurities in the organic solvent. Any traces of water would lead to agglomeration of the GLAD pillars. XPS spectra confirms the attachment of the organic moieties to the

surface of GLAD film. Following surface functionalisation, all GLAD films were rendered extremely hydrophobic as indicated by advancing aqueous contact angle measurements. The electrochemical studies of the siloxane-derivatised silica film also suggest that the siloxane reagents penetrates effectively into the GLAD film to tailor the interior surfaces of the pillars. Thus, a three-dimensional network of columnar nanostructures with controlled surface chemistry is produced.

To eliminate the detrimental effects of solvents on the structure of GLAD films (*e.g.*, agglomeration of the pillars), surface treatment methods were extended to vapour-phase functionalisation. The surface chemistry of a variety of metal oxide GLAD films (silica, titania, and alumina) were tailored through both solution and vapour-phase functionalisation methods. SEM micrographs confirmed that the GLAD nanostructures stayed intact throughout both functionalisation procedures for all metal oxide films, with the exception of vapour-phase-derivatised alumina. The voids of vapour-phase siloxane-tethered alumina film appeared to be completed impregnated as a result of the chemical byproduct reacting with the film. XPS spectra further confirmed this presumption by showing a significant decrease in aluminum and oxygen emissions in the vapour-phase siloxane-derivatised alumina film. However, it was demonstrated that alumina GLAD films can still be effectively vapour-phase functionalised with no structural changes if the reagent used did not produce byproducts that reacted with the film. Advancing aqueous contact angle measurements established that vapour-phase functionalisation method was a more straighforward and effective method for tailoring the surface chemistry of metal oxide GLAD films because it yields more uniform hydrophobic surfaces. However, regardless of the surface functionalisation methods applied, by combining the controlled surface chemistry with high porosity, large surface area GLAD nanostructures, extremely hydrophobic surfaces were created whose hydrophobicity exceeds their flat counterparts.

Finally, GLAD films with controlled surface chemistry was applied to GLAD-based capacitive humidity sensors. By rendering the sensor surface hydrophobic using previously described surface functionalisation methods, water adsorption was completely inhibited at all humidity levels. The capacitance of the chemical treated sensor remained relatively constant regardless of the changes in humidity. Clearly, a hydrophobic sensor does

not have an affinity for water, and thus becomes insensitive to all humidity changes in its environment. This phenomenon was later applied to an optical band-pass rugate filter fabricated using an advanced GLAD technique. Optical measurements of the functionalised filter demonstrated that by rendering its surface hydrophobic, the position of the pass band became desensitized to variations in humidity. Hence, by controlling the surface chemistry of GLAD films, optimal performance of the band-pass filter can be achieved independent of variations in humidity. In the future, the ability to tune and control the surface chemistry of GLAD films can be applied in the fabrication of GLAD-based chemical sensors via introducing selectivity for the compound to be detected. In addition, it can also enhanced the optical activity in helical structured GLAD films by tailoring the surface energy mismatch between liquid crystals and the substrate.

There are many promising applications for controlling the surface chemistry of GLAD with chemical functionalisation techniques, and a countless amount of further exploration and research is need to realise those potential applications. Much of the fundamental research for controlling the surface properties of GLAD films through effective tailoring of metal oxide GLAD films' surface chemistry via two straightforward, well-established, inexpensive surface functionalisation techniques has been provided in this thesis. Hence, the work presented in this thesis has made GLAD even more versatile by adding a chemical dimension to the tunability of GLAD films.

Bibliography

[1] M. Faraday, "The Bakerian lecture: Experimental relations of gold (and other metals) to light", *Phil. Trans.,* **147**, 145-181, (1857).

[2] R. Nahrwold, "The Bakerian lecture: Experimental relations of gold (and other metals) to light", *Ann. Physik.,* **31**, 467, (1887).

[3] A. Kundt, "The Bakerian lecture: Experimental relations of gold (and other metals) to light", *Ann. Physik.,* **147**, 145-181, (1888).

[4] R. Glang, in *Handbook of Thin Film Process Technology,* eds. L. I. Maissel and R. Glang, McGraw-Hill, New York (1970).

[5] E. B. Graper, "Evaporation characteristics of materials from an electron-beam gun", *J. Vac. Sci. Technol.,* **8**, 333-337, (1971).

[6] B. N. Chapman, *Glow Discharge Processes,* Wiley, New York (1980).

[7] W. A. Bryant, "The fundamentals of chemical vapour deposition", *J. Mater. Sci.,* **12**, 1285-1306, (1977).

[8] H. Pierson, *Handbook of Chemical Vapour Deposition: Principles, Technology and Applications,* Noyes Publications, New York (1992).

[9] T. Bando, and H. Sugiyama, "The chemical biology that controls DNA function and structure", *J. Synthet. Organ. Chem. Japan,* **63**, 1016-1027, (2005).

[10] Y. Xiao, P. E. Barker, "Semiconductor nanocrystal probes for human chromosomes and DNA", *Minerva Biotechnologica,* **16**, 275-282, (2004).

[11] K. R. Calvo, L. A. Liotta, and E. F. Petricoin, "Clinical proteomics: From biomarker discovery and cell signaling profiles to individualized personal therapy ", *Biosci. Rep.*, **25**, 107-125, (2005).

[12] D. F. Kong, and P. J. Goldschmidt-Clermont, "Tiny solutions for giant cardiac problems", *Trend. Cardiovascul. Med.*, **15**, 207-211, (2005).

[13] X. L. Ren, X. M. Meng, and F. Q. Tang, "Preparation of Ag-Au nanoparticle and its application to glucose biosensor", *Sensor Actuat. B,* **110**, 382-389, (2005).

[14] A. Kahru, A. Ivask, K. Kasemets, L. Pollumaa, I. Kurvet, M. Francois, and H. C. Dubourguier, "Biotests and biosensors in ecotoxicological risk assessment of field soils polluted with zinc, lead, and cadmium", *Environ. Toxic. Chem.*, **24**, 2973-2982, (2005).

[15] S. Srivastava, P. Singh, R. Bhagat, and V. N. Tripathi, "Application of bacterial biomass as a potential metal indicator", *Curr. Sci.*, **89**, 1248-1251, (2005).

[16] D. Vuillaume, "Nanometer-scale organic thin film transistors from self-assembled monolayers", *J. Nanosci. Nanotechnol.*, **2**, 267-279, (2002).

[17] J. Lehmann, S. Camalet, S. Kohler, and P. Hanggi, "Laser controlled molecular switches and transistors", *Chem. Phys. Lett.*, **368**, 282-288, (2003).

[18] A. Javey, J. Guo, D. B. Farmer, Q. Wang, E. Yenilmez, R. G. Gordon, M. Lundstrom, and H. J. Dai, "Self-aligned ballistic molecular transistors and electrically parallel nanotube arrays", *Nano Lett.*, **4**, 1319-1322, (2004).

[19] C. F. O. Graeff, G. B. Silva, F. Nuesch, and L. Zuppiroli, "Transport and recombination in organic light-emitting diodes studied by electrically detected magnetic resonance", *Europ. Phys. J. E,* **18**, 21-28, (2005).

[20] J. G. C. Veinot, and T. J. Marks, "Toward the ideal organic light-emitting diode. The versatility and utility of interfacial tailoring by cross-linked siloxane interlayers", *Acc. Chem. Res.*, **38**, 632-643, (2005).

[21] A. P. Kulkarni, C. J. Tonzola, A. Babel, S. A. Jenekhe, "Electron transport materials for organic light-emitting diodes", *Chem. Mater.*, **16**, 4556-4573, (2004).

[22] D. R. Solli, and J. M. Hickmann, "Photonic crystal based polarization control devices", *J. Phys. D - Appl. Phys.*, **37**, R263-R268, (2004).

[23] M. Perrin, S. Fasquel, T. Decoopman, X. Melique, O. Vanbesien, E. Lheurette, and D. Lippens, "Left-handed electromagnetism obtained via nanostructured metamaterials: comparison with that from microstructured photonic crystals", *J. Opt. A,* **7**, S3-S11, (2005).

[24] S. V. Patel, T. E. Mlsna, B. Fruhberger, E. Klaassen, S. Cemalovic and D. R. Baselt, "Chemicapacitive microsensors for volatile organic compound detection", *Sensor. Actuat. B,* **96**, 541-553, (2003).

[25] L. Holland, "The effect of vapour incidence on the structure of evaporated aluminum films", *J. Opt. Soc. Am.*, **43**, 376-380, (1953).

[26] N. O. Young, and J. Kowal, "Optically active fluorite films", *Nature,* **183**, 104-105, (1959).

[27] T. Motohiro, and Y. Taga, "Thin film retardation plate by oblique deposition", *Appl. Opt.*, **28**, 2466-2482, (1989).

[28] D. O. Smith, "Anisotropy in permalloy films", *J. Appl. Phys.*, **30**, 264S-265S, (1959).

[29] D. O. Smith, M. S. Cohen, and G. P. Weiss, "Oblique-incidence anisotropy in evaporated permalloy films", *J. Appl. Phys.*, **31**, 1755-1762, (1960).

[30] M. S. Cohen, "Anisotropy in permalloy films evaporated at grazing incidence", *J. Appl. Phys.*, **32**, 87S-88S, (1961).

[31] K. Robbie, and M. J. Brett, "First thin film realization of a helicoidal bianisotropic medium", *J. Vac. Sci. Technol. A,* **13**, 2991-2993, (1995).

[32] M. D. Arnold, I. J. Hodgkinson, Q. H. Wu, and R. J. Alaikie, "Multi-axis retarder arrays by masked oblique deposition", *J. Vac. Sci. Technol. B,* **23**, 1398-1404, (2005).

[33] I. J. Hodgkinson, Q. H. Wu, L. De Silva, M. Arnold, M. W. McCall, and A. Lahtakia, "Supermodes of chiral photonic fliters with combined twist and layer defects", *Phys. Rev. Lett.,* **91**, 223903/1-4, (2003).

[34] F. Wang, and A. Lakhtakia, "Defect modes in multisection helical phtonic crystals", *Opt. Exp.,* **13**, 7319-7335, (2005).

[35] A. Lakhtakia, M. W. McCall, J. A. Sherwin, Q. H. Wu, and I. J. Hodgkinson, "Sculptured-thin-film spectral holes for optical sensing of fluids", *Opt. Comm.,* **194**, 33-46, (2001).

[36] J-G Fang, and Y-P Zhao, "Water contact angles of vertically aligned Si nanorod arrays", *Nanotechnology,* **15**, 501-504, (2004).

[37] J-G Fang, D. Dyer, G. Zhang, and Y-P Zhao, "Nanocarpet effect: pattern formation during the wetting of vertically aligned nanorod arrays", *Nano Lett.,* **4**, 2133-2138, (2004).

[38] M. O. Jensen, and M. J. Brett, "Porosity engineering in glancing angle deposition thin films", *App. Phys. A,* **80**, 763-768, (2005).

[39] M. O. Jensen, S. R. Kennedy, and M. J. Brett, "Fabrication of periodic arrays of nanoscale square helices", *Mater. Res. Soc.,* **728**, 203-208, (2002).

[40] M. O. Jensen, and M. J. Brett, "Functional pattern engineering in glancing angle deposition thin films", *J. Nanosci. Nanotech.,* **10**, 1-6, (2005).

[41] S. R. Kennedy, and M. J. Brett, "Advanced techniques for the fabrication of square spiral phtonic crystals", *J. Vac. Sci. Technol. B,* **22**, 1184-1190, (2004).

[42] A. C. van Popta, M. M. Hawkeye, J. C. Sit, and M. J. Brett, "Gradient-index narrow-bandpass filter fabricated with glancing-angle deposition", *Opt. Lett.,* **29**, 2545-2547, (2004).

[43] K. D. Harris, J. R. McBride, K. E. Nietering, and M. J. Brett, "Fabrication of porous platinum thin films for hydrocarbon sensor applications", *Sens. Mater.,* **13**, 225-234, (2001).

[44] J. J. Steele, K. D. Harris, and M. J. Brett, "Nanostructured oxide films for high-speed humidity sensors", *Mater. Res. Soc.,* **788**, 473-477, (2004).

[45] E. B. Graper, *Handbook of Thin Film Process Technology,* A1.2:1-A1.2:12, (1995).

[46] J. F. O'Hanlon, *A User's Guide to Vacuum Technology,* John Wiley and Songs Inc., (1980).

[47] M. Ohring, *The Materials Science of Thin Films,* 263-264, Academic Press, (1992).

[48] L. Abelmann, and C. Lodder, "Oblique deposition and surface diffusion", *Thin Solid Films,* **305**, 1-21, (1997).

[49] A. Movchan, and A. V. Demchishin, "Study of the structure and properties of thick vacuum condensates of nickel, titanium, tungsten, aluminium oxide and zirconium oxide", *Phys. Met. Metallog.,* **28**, 83-90, (1969).

[50] J. A. Thronton, "High-rate thick film growth", *Ann. Rev. Mater. Sci.,* **7**, 239-260, (1977).

[51] R. Messier, A. P. Giri, and R. A. Roy, "Revised structure zone model for thin film physical structure", *J. Vac. Sci. Technol. A,* **2**, 500-503, (1984).

[52] R. Messier, "Towards quantification of thin film morphology", *J. Vac. Sic. Technol. A,* **4**, 490-495, (1986).

[53] J. M. Nieuwenhuizen, and H. B. Haanstra, "Microfractography of thin films", *Philips Tech. Rev.,* **27**, 87-91, (1966).

[54] R. N. Tait, T. Smy, and M. J. Brett, "Modelling and characterization of columnar growth in evaporated films", *Thin Solid Films,* **226**, 196-201, (1993).

[55] S. R. Kennedy, and M. J. Brett, "Porous broadband antireflection coating by glancing angle deposition", *Appl. Opt.*, **42**, 4573-4579, (2003).

[56] M. Seto, K. Westra, and M. Brett, "Arrays of self-sealed microchambers and channels", *J. Mater. Chem.*, **12**, 2348-2351, (2002).

[57] J. Cui, Q. Huang, J. G. C. Veinot, H. Yan, and T. J. Marks, "Interfacial microstructure function in organic light-emitting diodes: assembled tetraaryldiamine and copper phthalocyanine interlayers", *Adv. Mater.*, **14**, 565-569, (2002).

[58] A. Ulman, *An Introduction to Ultrathin Organic Films: From Langmuir-Blodgett to Self-Assembly,* American Press, New York, 1988

[59] G. L. Gaines Jr., *Insoluble Monolayers at Liquid-Gas Interfaces,* Interscience, New York, 1966.

[60] C. D. Bains, and G. M. Whitesides, "Modeling organic surfaces with self-assembled monolayers", *Angew. Chem. Int. Ed. Engl.*, **28**, 506-512, (1989).

[61] J. E. Malinsky, J. G. C. Veinot, G. E. Jabbour, S. E. Shaheen, J. D. Anderson, P. Lee, A. G. Richter, A. L. Burin, M. A. Ratner, T. J. Marks, N. R. Armstrong, B. Kippelen, P. Dutta, and N. Peyghambarian, "Nanometer-scale dielectric self-assembly process for anode modification in organic light-emitting diodes. Consequences for charge injection and enhanced luminous efficiency", *Chem. Mater.*, **14**, 3054-3065, (2002).

[62] H. M. Shang, Y. Wang, S. J. Limmer, T. P. Chou, K. Takahashi, and G. Z. Cao, "Optically transparent superhydropobic silica-based films", *Thin Solid Films,* **472**, 37-43, (2005).

[63] S. Flink, F. C. J. M. Van Veggel, and D. N. Reinhoudt, "Sensor functionalities in self-assembled monolayers", *Adv. Mater.*, **12**, 1315-1328, (2000).

[64] T. Wink, S. J. Van Zuilen, S. J. Bult, and W. P. van Bennekom, "Self-assembled monolayers for biosensors", *Analyst,* **122**, 43R-45R, (1997).

[65] C. Duan, and M. E. Meyerhoff "Separation-free sandwich enzyme immunoassay using microporous gold electrodes and self-assembled monolayer/immobilized capture antibodies", *Anal. Chem.*, **66**, 1369-1377, (1994).

[66] S. Virji, J. Huang, R. B. kaner, and B. H. Weiller, "Polyaniline nanofiber gas sensors: examination of response mechanisms", *Nano Lett.*, **4**, 491-496, (2004).

[67] I. Langmuir, "The constitution and fundamental properties of solids and liquids. II. ", *J. Am. Chem. Soc.*, **39**, 1849-1906, (1917).

[68] A. Pockels, "The tension of composite fluid surfaces and the mechanical stability of films of fluid", *Nature,* **50**, 223, (1894).

[69] W. B. Hardy, "The tension of composite fluid surfaces and the mechanical stability of films of fluid", *Proc. R. Soc. London A,* **86**, 610-635, (1912).

[70] K. B. Blodgett, "Films built by depositing successive monomolecular layers on a solid surface ", *J. Am. Chem. Soc.*, **57**, 1007-1022, (1935).

[71] S. R. Forrest, "Ultrathin organic films grown by organic molecular beam deposition and related techniques", *Chem. Rev.*, **97**, 1793-1896, (1997).

[72] E. Umbach, M. Sokolowski, and R. Fink, "Substrate-interaction, long-range order, and epitaxy of large organic adsorbates", *Appl. Phys. A,* **63**, 565-576, (1996).

[73] P. Tecilla, P. R. Dixon, G. Slobodkin, D. S. Alavi, D. H. Waldeck, and A. D. Hamilton, "Hydrogen-bonding self-assembly of multichromophore strucures", *J. Am. Chem. Soc.*, **112**, 9408, (1990).

[74] Y. Koide, M. W. Such, R. Basu, G. Evmenenko, J. Cui, P. Dutta, M. C. Hersam, and T. J. Marks, "Hot microcontact printing for patterning ITO surfaces. Methodology, morphology, microstructure, and OLED charge injection barrier imaging", *Langmuir,* **19**, 86-93, (2003).

[75] P. M. St. John, and J. G. Craighead, "Microcontact printing and pattern transfer using trichlorosilanes on oxide substrates", *Appl. Phys. Lett.*, **68**, 1022-1024, (1996).

[76] Y. Xia, M. Mrksich, E. Kim, and G. M. Whitesides, "Microcontact printing of octadecylsiloxane on the surface of silicon dioxide and its application in microfabrication", *J. Am. Chem. Soc.*, **117**, 9576-9577, (1995).

[77] R. Maoz, E. Frydman, S. R. Cohen, and J. Sagiv, "Constructive nanolithography: site-defined silver self-assembly on nanoelectrochemically patterned monolayer templates", *Adv. Mater.*, **12**, 424-429, (2000).

[78] S. Liu, R. Maoz, G. Schmid, and J. Sagiv, "Template guided self-assembly of [Au_{55}] clusters on nanolithographically defined monolayer patterns", *Nano Lett.*, **2**, 1055-1060, (2002).

[79] S. Hoeppener, R. Maoz, S. R. Cohen, L. Chi, H. Fuchs, and J. Sagiv "Metal nanoparticles, nanowires, and contact electrodes self-assembled on patterned monolayer templates-a bottom-up chemical approach", *Adv. Mater.*, **14**, 1036-1041, (2002).

[80] H. Yan, Q. Huang, J. Cui, J. G. C. Veinot, M. M. Kern, and T. J. Marks, "High-brightness blue light-emitting polymer diodes via anode modification using a self-assembled monolayer", *Adv. Mater.*, **15**, 835-838, (2003).

[81] P. Zhu, M. E. van der Boom, H. Kang, G. Evmenenko, P. Dutta, and T. J. Marks, "Realization of Expeditious Layer-by-Layer Siloxane-Based Self-assembly as an Efficient Route to Structurally Regular Acentric Superlattices with Large Electro-optic Responses", *Chem. Mater.*, **14**, 4982-4989, (2002).

[82] N. G. Semaltianos, J.-L. Pastol, and P. Doppelt, "Copper nucleation by chemical vapour deposition on organosilane treated SiO_2 surfaces", *Surf. Sci.*, **562**, 157-169, (2004).

[83] N. E. Cant, K. Critchley, H.-L. Zhang, S. D. Evans, "Surface functionalisation for the self-assembly of nanopartical/polymer multilayer", *Thin Solid Films*, **426**, 31-39, (2003).

[84] L. H. Dubois, and B. R. Zegarski, "Molecular ordering of organosulfur compounds on Au(111) and Au(110): adsorption from solution and in ultrahigh vacuum", *J. Chem. Phys.*, **98**, 678-688, (1993).

[85] G. E. Poirier, "Coverage-dependent phases and phase stability of decanethiol on Au(111) ", *Langmuir,* **15**, 1167-1175, (1999).

[86] F. Schreiber, A. Eberhardt, T. Y. B. Leung, P. Schwartz, S. M. Wetterer, D. J. Lavrich, L. Berman, P. Fenter, P. Eisenberger, and G. Scoles, "Adsorption mechanisms, structures, and growth regimes of an archetypal self-assembling system: decanethio on Au(111)", *Phys. Rev. B,* **57**, 12476-12481, (1998).

[87] P. Schwartz, F. Schreiber, P. Eisenberger, and G. Scoles, "Growth kinetics of decanethiol monolayers self-assembled on Au(111) by molecular beam deposition: an atomic beam diffraction study", *Surf. Sci.,* **423**, 208-224, (1999).

[88] J-B Lhuillier, C. Martin, L. Ressie, J. P. Peyrade, J. Grisolia, and M. Respaud, "Elaboration of 1μm square arrays of octadecyltrimethoxysilane monolayers on SiO_2/Si by combining chemcial vapour deposition an dnano-imprint lithography", *Superlattice Microst.,* **36**, 227-223, (2004).

[89] P. Doppelt, and M. Stelzle, "Selective metallizatin of silica surfaces by copper CVD using a chemical affinity pattern created by gas phase silylation and UV exposure", *Microelectron. Eng.,* **33**, 15-23, (1997).

[90] S. Li, H. Li, X. Wang, Y. Song, Y. Liu, L. Jiang, and D. Zhu, "Superhydrophobicity of large-area honeycomb-like aligned carbon nanotubes", *J. Phys. Chem. B,* **106**, 9274-9276, (2002).

[91] T. Sun, L. Feng, X. Gao, and L. Jiang, "Bioinspired surfaces with special wettability", *Acc. Chem. Res.,* **38**, 644-652, (2005).

[92] X. Feng, L. Feng, M. Jin, J. Zhai, L. Jiang, and D. Zhu, "Reversible super-hydrophobicity to super-hydrophilicity transition of aligned ZnO nanorod films", *J. Am. Chem. Soc.,* **126**, 62-63, (2004).

[93] X. Zhang, F. Shi, X. Yu, H. Liu, Y. Fu, Z. Wang, L. Jiang, and X. Li, "Polyelectrolyte multilayer as matrix for electrochemical deposition of gold clusters: toward super-hydrophobic surface", *J. Am. Chem. Soc.,* **126**, 3064-3065, (2004).

[94] D.-H. Jung, I. J. Park, Y. K. Choi, S.-B. Lee, H. S. Park, and J. Rühe, "Perfluorinated polymer monolayers on porous silica for materials with super liquid repellent properties", *Langmuir,* **18**, 6133-6139, (2002).

[95] D. O. H. Teare, C. G. Spanos, P. Ridley, E. J. Kinmond, V. Roucoules, and J. P. S. Badyal, "Pulsed plasma deposition of super-hydrophobic nanospheres", *Chem. Mater.,* **14**, 4566-4571, (2002).

[96] J. C. Sit, "Thin film/liquid crystal composite optical materials and devices", Ph. D. dissertation, University of Alberta, Canada, (2002).

[97] S. R. Kennedy, "Applications of nanostructured thin films", Ph. D. dissertation, University of Alberta, Canada, (2003).

[98] K. Robbie, J. C. Sit, and M. J. Brett, "Advanced techniques for glancing angle deposition", *J. Vac. Sci. Technol. B,* **16**, 1115-1122, (1998).

[99] K. Robbie, and M. J. Brett, "Sculptured thin films and glancing angle deposition: growth mechanics and applications", *J. Vac. Sci. Technol. A,* **15**, 1460-1465, (1997).

[100] K. Robbie, C. Shafai, and M. J. Brett, "Thin films with nanometer-scale pillar microstructure", *J. Mater. Res.,* **14**, 3158-3163, (1999).

[101] Z. Bacsik, J. Mink, and G. Keresztury, "FTIR spectroscopy of the atmosphere I. Principles and Methods", *App. Spec. Rev.,* **39**, 295-363, (2004).

[102] D. H. Williams and I. Fleming, *Spectroscopic Methods in Organic Chemistry,* McGraw-Hill, London, 1995

[103] S. Hoeppener, R. Maoz, and J. Sagiv, "Constructive microlithography: electrochemical printing of monolayer template paterns extends constructive

nanolithography to the micrometer-millimeter dimension range", *Nano Lett.*, **3**, 761-767, (2003).

[104] R. Maoz, E. Frydman, S. R. Cohen, and J. Sagiv, "Constructive nanolithography: inert monolayers as patternable templates for in-situ nanofabrication of metal-semiconductor-organic surface structures-a generic appraoch", *Adv. Mater.*, **12**, 725-731, (2000).

[105] S. Liu, r. Maoz, and J. Sagiv, "Planned nanostructures of colloidal gold via self-assembly on hierarchically assembled organic bilayer template patterns with in-situ generated terminal amino functionality", *Nano Lett.*, **4**, 845-851, (2002).

[106] J. Cui, Q. Huang, J. G. C. Veinot, H. Yan, Q. Wang, G. R. Hutchison, A. G. Richter, G. Evmenenko, P. Dutta, and T. J. Marks, "Anode interfacial engeineering appraoches to enhancing anode/hole transport layer interfacial stability and charge injection efficiency in organic light-emitting diodes", *Langmuir,* **18**, 9958-9970, (2002).

[107] S. J. Geng, S. Zhang, and H. Onishi, "XPS applications in thin films research", *Mater. Tech.*, **17**, 234-240, (2002).

[108] M. P. Seah, "A review of the analysis of surfaces and thin films by AES and XPS", *Vaccum,* **34**, 463-478, (1984).

[109] S. Tsoi, E. Fok, J. C. Sit, J. G. C. Veinot, "Superhydrophobic, high surface area, 3-D SiO_2 nanostructures through siloxane-based surface functionalization", *Langmuir,* **20**, 10771-10774, (2004).

[110] T. Young, "An essay on the cohesion of fluids", *Philos. Trans. R. Soc. London,* **95**, 65-87, (1805).

[111] D. Y. Kwok "Contact angles: measurements, interpretation, adhesion and molecular theory", *Rec. Res. Devel. Physical Chem.*, **6**, 651-720, (1996).

[112] R. N. Wenzel, "Resistance of solid surfaces to wetting by water", *Ind. Eng. Chem.*, **28**, 988-994, (1936).

[113] A. B. D. Cassie, and S. Baxter, "Wettability of porous surfaces", *Trans. Faraday Soc.*, **40**, 546-551, (1944).

[114] J. Heinze, "Cyclic voltammetry-electrochemical spectroscopy", *Angew. Chem. Int. Edt.*, **23**, 831-918, (1984).

[115] B. Speiser, "From cyclic voltammetry to scanning electrochemical microscopy: modern electroanalytical methods to study organic compounds, materials and reations", *Curr. Org. Chem.*, **3**, 171-191, (1999).

[116] W. R. Thompson,and J. E. Pemberton, "Characterization of cctadecylsilane and stearic acid layers on Al_2O_3 surfaces by raman spectroscopy", *Langmuir,* **11**, 1720-1725, (1995).

[117] N. L. Jeon, K. Finnie, K. Branshaw, and R. G. Nuzzo, "Structure and stability of patterned self-assembled films of octadecyltrichlorosilane formed by contact printing", *Langmuir,* **13**, 3382-3391, (1997).

[118] P. M. Visintin, R. G. Carbonell, C. K. Schauer, and J. M. DeSimone, "Chemical Functionalization of Silica and Alumina Particles for Dispersion in Carbon Dioxide", *Langmuir,* **21**, 4816-4823, (2005).

[119] M. Advincula, X. Fan, J. Lemons, and R. Advincula, "Surface modification of surface solVgel derived titanium oxide films by self-assembled monolayers (SAMs) and non-specific protein adsorption studies", *Collid. Surface B,* **42**, 29, (2005).

[120] K. D. Harris, A. Huizinga, and M. J. Brett, "High-speed porous thin film humidity sensors", *Electrochem. Solid. Stat.*, **5**, H27-H29, (2002).

[121] K. D. Harris, A. Huizinga, and M. J. Brett, "A simple and inexpensive humidity control chamber", *Meas. Sci. Techno.*, **13**, N10-N11, (2002).

[122] J. J. Steele, S. Tsoi, J. Gospodyn, J. G. C. Veinot, J. C. Sit, and M. J. Brett, "Surface functionalization and porosity studies of high-speed humidity sensors", *Proc. IEEE Sens.*, **2**, 760-763, (2004).

[123] A. C. van Popta, S. R, Kennedy, D. J. Broer, J. C. Sit, and M. J. Brett, "Optical performances of porous TiO_2 chiral thin films", *Proc. SPIE,* **5213**, 232-241, (2003).